Midcell localization of PBP4 of *Escherichia coli* modulates the timing of divisome assembly

Jolanda Verheul[1#], Adam Lodge[2,7#], Hamish C.L. Yau[2,8#], Xiaolong Liu[1,9#], Xinwei Liu[1], Alexandra S. Solovyova[3], Athanasios Typas[4,5] Manuel Banzhaf[6*], Waldemar Vollmer[2**], and Tanneke den Blaauwen[1***]

[1]Bacterial Cell Biology, Swammerdam Institute for Life Sciences, Faculty of Science, University of Amsterdam; Science Park 904, 1098 XH Amsterdam, The Netherlands.
[2]Centre for Bacterial Cell Biology, Biosciences Institute, Newcastle University, Newcastle upon Tyne, NE2 4AX, United Kingdom.
[3]NUPPA, Leech Building, Framlington Place, Newcastle upon Tyne NE2 4HH, UK
[4]European Molecular Biology Laboratory, Genome Biology Unit, Heidelberg, Germany
[5]European Molecular Biology Laboratory, Structural & Computational Unit, Heidelberg, Germany
[6]Institute of Microbiology & Infection and School of Biosciences, University of Birmingham, Edgbaston, Birmingham, UK. B15 2TT
[7]Present address: Iksuda Therapeutics, The Biosphere, Draymans Way, Newcastle Helix, Newcastle upon Tyne, NE4 5BX, UK
[8]Pressent address: Procter & Gamble, Newcastle Innovation Centre, Whitley Road, Newcastle-Upon Tyne, NE12 9TS, UK.
[9]Department of Biochemistry, University of Oxford, OX1 3QU, Oxford, United Kingdom.

[#]contributed equally.
*Corresponding author. Tel: +44 121 4145586; Email: m.banzhaf@bham.ac.uk
**Corresponding author. Tel: +44 191 208 3216; Email: w.vollmer@ncl.ac.uk
***Corresponding author. Tel: +31 20 525 3852; Email: t.denblaauwen@uva.nl

Running title: PBP4 modulates divisome assembly

ABSTRACT (176 words)

Insertion of new material into the *Escherichia coli* peptidoglycan (PG) sacculus between the cytoplasmic membrane and the outer membrane requires a well-organized balance between synthetic and hydrolytic activities to maintain cell shape and avoid lysis. The hydrolytic enzymes outnumber the enzymes that insert new PG by far and very little is known about their specific function. Here we show that the DD-carboxy/endopeptidase PBP4 localizes in a PBP1A/LpoA and FtsEX dependent fashion at midcell during septal PG synthesis. Midcell localization of PBP4 requires its non-catalytic domain 3 of unknown function, but not the activity of PBP4 or FtsE. Microscale thermophoresis with isolated proteins shows that domain 3 is needed for the interaction with NlpI, but not PBP1A or LpoA. *In vivo* crosslinking

experiments confirm the interaction of PBP4 with PBP1A and LpoA. We propose that PBP4 functions together with the amidases AmiA and B to create denuded glycan strands to attract the initiator of septal PG synthesis, FtsN. Consistent with this model, we found that the divisome assembly at midcell was significantly affected in cells lacking PBP4.

IMPORTANCE (140 words)

Peptidoglycan biosynthesis is a major target for antibacterials. The covalently closed peptidoglycan mesh, called sacculus, protects the bacterium from lysis due to its turgor. Sacculus growth is facilitated by the balanced activities of synthases and hydrolases, and disturbing this balance leads to cell lysis and bacterial death. Because of the large number and possible redundant functions of peptidoglycan hydrolases, it has been difficult to decipher their individual functions. In this paper we show that the DD-endopeptidase PBP4 localizes at midcell during septal peptidoglycan synthesis in *Escherichia coli* and is important for the timing of the assembly of the division machinery. This shows that inhibition of certain hydrolases could weaken the cells and might enhance antibiotic action.

KEYWORDS: bacterial cell division, endopeptidase, immunolabeling, LpoA, NlpI, PBP1A, PBP4, peptidoglycan, preseptal, protein interactions

INTRODUCTION

The peptidoglycan (PG) layer is sandwiched between the cytoplasmic membrane (CM) and the outer membrane (OM) of the Gram-negative bacterium *Escherichia coli* forming a covalently closed network of glycan strands that are interconnected by short peptides [1]. The PG layer maintains the shape of the bacterium by stabilizing the cell against its high

66 internal osmotic pressure. To proliferate, the rod-shaped bacterium grows in length and then
67 divides by binary fission into two equally sized daughter cells. The balanced activities of PG
68 synthases and hydrolases ensures a safe extension of the PG layer without defects that would
69 cause cell lysis [2]. Beta-lactam antibiotics disturb this balance by inactivating the
70 transpeptidase (TPase) activity of the penicillin binding proteins (PBP)s causing lysis of
71 growing cells. We currently know more than twenty PG hydrolases that can cleave either in
72 the glycan chains or peptides within the PG layer, but how their activities are regulated is
73 poorly understood. This is particularly true for the PG endopeptidases [2]. Recently, the OM
74 bound lipoprotein NlpI was shown to interact with similar affinity with several
75 endopeptidases, suggesting that NlpI acts as an interaction hub for endopeptidases to
76 regulate their activities by competing protein-protein interactions. [3].

77 The basic precursor (lipid II) for PG synthesis is the β-(1,4) linked disaccharide *N*-
78 acetylglucosamine-*N*-acetylmuramic acid (Glc*N*Ac-Mur*N*Ac) with an undecaprenol-
79 pyrophosphate linked to C1 of Mur*N*Ac and a stem peptide with the sequence L-alanine-D-
80 *iso*-glutamate-diaminopimelic acid (Dap)-D-alanine-D-alanine coupled to the C3 of Mur*N*Ac.
81 Lipid II is used by glycosyltransferases (GTases), which polymerize the glycan chains, and
82 TPase, which crosslink the stem peptides. The main PG synthases in *E. coli* are the class A PBPs
83 (PBP1A and PBP1B) with GTase and TPase activities [4–8], the integral membrane proteins
84 RodA and FtsW with GTase activity [9–11] and their partner TPases PBP2 and PBP3,
85 respectively [12–15].

86 The hydrolases are present in greater redundancy than the synthases [2,16]. The
87 carboxypeptidases (CPase) PBP5, PBP6A and PBP6B remove the terminal D-Ala from nascent
88 pentapeptides [17–20]. The endopeptidases (EPases) PBP4, PBP7, MepA, MepM, MepH, and
89 MepS cleave the crosslinks in the PG [21–23]. The amidases AmiA-D hydrolyze the bond

90 between Mur*N*Ac and L-alanine at position 1 of the stem peptide [24–27]. Finally, the lytic
91 transglycosylases Slt70 and MltA-G cleave the glycan strands to release 1,6-anhydroMur*N*Ac
92 containing turnover products [28–30]. The large number of hydrolases reflects the
93 adaptability to various environmental conditions {Pazos; Muellersw} but begs the question of
94 how their potentially dangerous activities are controlled to avoid cell lysis.

95 Binary fission in *E. coli* is initiated by the assembly of the Z-ring at midcell, which
96 consist of a network of dynamic FtsZ filaments that are anchored to the cytoplasmic
97 membrane by FtsA and ZipA [31,32]. The Z-ring also recruits the PG synthases PBP1A and
98 PBP1B to midcell [4,33]. A number of Z-associated proteins play a role in the organization and
99 dynamics of the ring [34–39]. Of these, the integral membrane protein FtsX interacts with
100 FtsA [40] and its cytoplasmic ATPase partner protein FtsE interacts with FtsZ [41]. Both localize
101 early to midcell, together with the Z-ring [24]. As a complex FtsEX recruits EnvC, which
102 activates AmiA and AmiB that are needed for septum cleavage [26,42]. FtsE versions without
103 ATPase activity still localize at midcell and recruit as FtsEX-EnvC complex but the latter is not
104 able to activate the amidases [43]. Presumably an ATPase dependent conformational change
105 in FtsEX induces a conformational change in EnvC, which is then able to relieve an
106 autoinhibitory alpha-helix from the active site of AmiA and AmiB, activating them [44]. The
107 third amidase AmiC is activated by the OM-anchored lipoprotein NlpD [24] and all three
108 amidases AmiA-C are activated under certain stress conditions by the recently identified ActS
109 [46,47]. The recruitment of the other cell division proteins occurs with a time delay of about
110 20% of the cell division cycle, depending on the growth condition [48–50]. FtsK, FtsBLQ, FtsW,
111 PBP3 and FtsN localize in an interdependent fashion. FtsBLQ inhibit the PG synthase activity
112 of PBP3, FtsW and PBP1B until they are outcompeted by the accumulation of FtsN that
113 relieves this inhibition and initiates septum synthesis [51–54].

114 While investigating the specific function of various PG hydrolases, we found that PBP4
115 localizes specifically at midcell as part of the division machinery. PBP4 is a periplasmic
116 endopeptidase [55] with a C-terminal amphipathic alpha-helix that associates with
117 membranes [56]. Deletion of *dacB*, which encodes PBP4, does not have morphological
118 consequences but causes a decrease in the percentage of PG crosslinks and of PG-attached
119 lipoprotein [57] and an increased sensitivity to bile salts [58]. Overproduction of PBP4 is toxic
120 [59] presumably because the enhanced cleavage of peptide cross-links weakens the PG mesh
121 and eventually causes lysis. PBP4 has three domains that are assembled in an unusual way
122 [60] (Fig. 1A). A non-catalytical domain of unknown function (domain 2) is inserted into the
123 transpeptidase domain 1, and a third domain (domain 3) is inserted into domain 2. Domain 3
124 is positioned above the active site with its catalytic serine 62, which resides in domain 1, and
125 might be involved in substrate binding or regulation [61] (Fig. 1A). Site directed mutagenesis
126 suggested that residues from domain 1 (R361) and 2 (D155) are important for the
127 endopeptidase activity [62].
128 Here we determined the localization of PBP4 and different variants during the cell
129 cycle of *E. coli.* The timing of localization at midcell and interactions of PBP4 support a role in
130 remodeling of PG synthesized by the divisome.
131
132 **RESULTS**
133
134 **PBP4 localizes to the lateral wall and at midcell.** To determine the localization of PBP4 in *E.*
135 *coli* cells as a function of the bacterial cell cycle, we generated an antiserum against PBP4 and
136 removed unspecific antibodies by adsorption to cells of a *dacB* deletion mutant that lacks
137 PBP4. The purified antibodies were specific for PBP4 (Fig. S1) and used to immunolabel the

138 wild-type strain MC4100 grown in rich (TY) medium at 37°C. PBP4 localized strongly at midcell
139 and to a lesser extend in the lateral wall in wild-type cells (Fig. 1B).

140 **PBP4 localizes between the peptidoglycan layer and the outer membrane**. Although
141 it was reported that PBP4 has a stretch of weakly amphipathic amino acids at its C-terminus
142 [56], it was not known whether PBP4 freely diffuses in the periplasm or associates with the
143 membrane or other proteins. It has been previously observed that chemically fixing freely
144 diffusing periplasmic proteins can shock them into the cell poles [12,63]. The fact that we did
145 not observe any polar localization of PBP4 after fixation (Fig. 1B and S1), suggests that it is
146 either associated with the membrane or other proteins. Next, we investigated whether PBP4
147 was accessible to anti-PBP4 in cells with an intact PG layer. For this, wild-type cells were grown
148 in TY at 37°C and immunolabeled without the typically used Triton X-100-mediated
149 permeabilization of the OM or without digesting the PG mesh with lysozyme. PBP4 was not
150 accessible without permeabilization of the OM but was fully accessible in cells with an intact
151 PG (Fig. 1C). In contrast, proteins like FtsN and PBP3 were not accessible without degradation
152 of the PG layer by lysozyme (Fig. 1C). The OM pore inserting BAM complex is also not
153 accessible without lysozyme treatment [64]. This suggests that PBP4 resides between the OM
154 and the PG layer.

155 **Activity of PBP4 is not needed for midcell localization.** Substrate binding can be a key
156 determinant in the localization of proteins [18,65,66]. To test whether PBP4 substrate binding
157 is needed to localize at division sites we expressed the active site mutants PBP4(S62G) and
158 (S62A) [61] that fails to bind β-lactams and therefore is not able to hydrolyze the PG stem
159 peptide (Fig. S2 and S3). A plasmid encoding the mutant protein was constitutively expressed
160 in a Δ*dacB* background by the leakage of a weakened p*Trc99*A promoter. Interestingly, the
161 wild-type and active site mutant when expressed from plasmid were both able to localize at

162 midcell (Fig. 2). This indicates that although PBP4(S62G) cannot hydrolyze its substrate or bind
163 β-lactams covalently (Fig. S2C Fig. S3), it is either still able to interact with its substrate or it
164 localizes through protein interactions.

165 Since PBP4(S62G) could still interact with its PG substrate, we mutagenized the gene
166 to express PBP4 versions in which residues D155 or R361 involved in the binding of the DAP
167 residue in the stem peptide by alanine [62] were replaced. The genes encoding PBP4(D155A)
168 or PBP4(R361A) were expressed by promoter leakage from plasmid in a Δ*dacB* background,
169 and both PBP4 versions localized at midcell (Fig. 2). An immunoblot analysis showed that all
170 mutants were expressed to similar levels and that PBP4(R361A) and PBP4(D155A) were able
171 to bind the fluorescent β-lactam Bocilin-FL (Fig. S2). Therefore, all three active site protein
172 variants are potentially able to interact with substrate as an inactive protein.

173 A PBP4 version lacking domain 3 (PBP4ΔD3) was still able to bind β-lactams (Fig. S2B
174 and S3) but did not have DD-carboxypeptidase or DD-endopeptidase activity (Fig. S3).
175 Analytical ultracentrifugation (Fig. S4A) and circular dichroism analysis (Fig. S4B) of isolated
176 PBP4ΔD3, showed that the removal of domain 3 did not affect the structure, the dimerization
177 of the rest of the protein or its interaction with PG sacculi (Fig. S4C), which suggests a folded
178 active site domain. However, although the inactive PBP4ΔD3 was capable of binding substrate,
179 it did not localize at midcell (Fig. 2). Hence, we conclude that the midcell localization of PBP4
180 is largely driven by protein-protein interactions and to a lesser extent by substrate interaction
181 but is independent from its own activity.

182 **PBP4 localizes at inactive divisomes.** To further dissect whether the localization of
183 PBP4 at the division site is dependent on the availability of its substrate or the presence of
184 other proteins at the division site, cell division was inhibited through the specific inactivation
185 of PBP3 by aztreonam [67]. Aztreonam treatment for 1-3 mass doublings stalls the division

186 machinery at midcell resulting in filamentous growth. In the longer filaments new division
187 machineries are formed and localize at future division sites [5]. In these filaments PBP4 still
188 localized albeit somewhat weaker than in untreated cells at all possible division sites (Fig. S5),
189 indicating that the activity of PBP3 was not required for the recruitment of PBP4. While PBP3
190 is inhibited, preseptal PG synthesis [68] still occurs at the potential division sites in the
191 filamenting cells [18,33,69]. The pre-septal localization of PBP4 mimics the localization of
192 PBP1A and PBP1B, which were previously shown to be recruited to preseptal PG synthesis
193 sites by early cell division proteins [4,33].

194 **PBP1A/LpoA assist in midcell localization of PBP4.** PBP4 was recently reported to
195 interact with PBP1A, LpoA and the EPase adaptor protein NlpI [3]. To investigate whether
196 PBP1A and/or LpoA proteins were needed for midcell localization of PBP4, strains deleted for
197 *mrcA* (PBP1A), *lpoA*, *mrcB* (PBP1B) or *lpoB* were grown in rich medium at 37°C and
198 immunolabeled with anti-PBP4. The amount of PBP4 that localized at midcell was identical
199 for the parental wild-type strain BW25113, Δ*mrcB* and Δ*lpoB,* but reduced in the Δ*mrcA* and
200 Δ*lpoA* strains (even after correction for the smaller diameter of these cells, [70], whereas the
201 PBP4 concentration was similar for all strains (Fig. 3). This could indicate that PBP1A/LpoA
202 assist in the initial localization of PBP4 at midcell.

203 **NlpI seems not to be involved in midcell localization of PBP4**. We next tested if the
204 interaction with the OM anchored NlpI affected the localization of PBP4. In the Δ*nlpI* cells the
205 amount of PBP4 at midcell per μm average cell circumference was reduced by 42 ± 6.7% (n =
206 3) of the wild type and the protein localized later at midcell than in the wild-type cells (Fig.
207 S6). However, the PBP4 concentration in the Δ*nlpI* strain was also lower than in the wild-type
208 cells (64.8 ± 17.6%, n = 3). This could indicate that the cells down-regulate PBP4 expression
209 or that PBP4 becomes unstable in the Δ*nlpI* strain. Labeling of PBP4 in a Δ*nlpI* strain did not

210 require lysozyme (Fig. S6), suggesting that NlpI is not needed to maintain PBP4 localized
211 outside the PG layer, which could be facilitated by additional interactions of PBP4.

212 **PBP4 domain 3 facilitates interaction with NlpI but not PBP1A/LpoA**. Microscale
213 thermophoresis (MST) in which one protein is labelled with a fluorophore and titrated with
214 an unlabeled partner protein was used to analyze the interactions between PBP4 and its
215 known interaction partners further. The difference in thermophoresis of the complex versus
216 the unbound fluorescently labeled proteins is then used to calculate the affinity of the binding
217 partners. Different versions of PBP4 and its interaction partners were purified and assayed
218 for direct protein-protein interactions. Wild-type PBP4 interacted with PBP1A, LpoA and NlpI
219 [3]. PBP4 lacking domain 3 (PBP4ΔD3), which did not localize at midcell (Fig. 2), still interacted
220 with PBP1A and LpoA but not with NlpI (Fig. 4). These results suggest that domain 3 of PBP4
221 facilitates the interaction with NlpI, but not PBP1A.

222 **NlpI and PBP1A/LpoA have different binding sites in PBP4.** PBP4 can form a multi-
223 enzyme complex with NlpI and PBP1A/LpoA [3]. PBP1A interacted with PBP4 and could be
224 cross-linked to PBP4 in cells (Fig. 4C). We found that full length LpoA interacted with both
225 PBP4 and PBP4ΔD3, with apparent K_D values of 315 ± 38 nM and 153 ± 31 nM, respectively
226 (Fig. 4A; Fig. S7). This suggests that domains 1 or 2 of PBP4 are sufficient for the interaction
227 with LpoA. MST assays of PBP4 or PBP4ΔD3 with LpoA's C-terminal (residues N257-S678;
228 $LpoA^C$) or N-terminal (LpoA residues G28-T256; $LpoA^N$) domains also yielded positive binding
229 curves (Fig. 4A; Fig. S7) [71–73]. We found that $LpoA^C$ and the full length LpoA version had
230 comparable affinities for both PBP4 versions, suggesting that the C-terminal domain of LpoA
231 is sufficient for interaction with PBP4 (Fig. 4A). Interestingly, the removal of domain 3 from
232 PBP4 resulted in an increased affinity of $LpoA^N$ for PBP4 (app. K_D decreased by ~50 fold) (Fig.
233 4A Fig. S7). Hence, the interaction between the N-terminal domain of LpoA and PBP4 possibly

234 occurs via a different mechanism dependent on a conformational rearrangement of domain
235 3 of PBP4. This suggests that the two domains of LpoA, which likely serve different primary
236 functions, are both sufficient for an interaction with PBP4, albeit with varying affinities. In
237 conclusion PBP4 robustly interacts with PBP1A/LpoA independent of its domain 3.

238 **LpoA has a small effect on PBP4 activity**. We found previously that NlpI does not
239 affect PBP4 activity [3] but considered it possible that PBP4 interaction with PBP1A/LpoA may
240 affect its activity. We first verified that NlpI or PBP4 did not affect the activity of PBP1A in the
241 presence or absence of LpoA using an *in vitro* glycosyltransferase assay (Fig. 5). We next
242 tested if PBP1A or LpoA affected the activity of PBP4 using *in vitro* PG degradation assays.
243 LpoA decreased the activity of PBP4 by about 30% in a continuous DD-CPase assay with
244 soluble substrate and an endpoint PG digestion assay (Fig 5B and C). To assess whether LpoA
245 also affects PBP4 activity *in vivo*, a Δ*dacB*Δ*lpoA* strain and Δ*dacB* strain were transformed
246 with the plasmids expressing PBP4 or the active site mutant PBP4(S62G) and the toxicity of
247 their expression was compared. Although the double mutant was less fit than the single
248 mutant, it was equally sensitive to the overexpression of PBP4 (Fig. 5D), leaving no indication
249 that LpoA also inhibits the activity of PBP4 *in vivo*.

250 **PBP4 localizes as early divisome protein.** Since PBP4 localizes at midcell it could be
251 part of or associated with the divisome. The division machinery is assembled in two successive
252 steps [48,74]. First, FtsZ and its membrane bound partners ZipA and FtsA in conjunction with
253 other Z-ring associated proteins form the proto-ring that localizes at midcell
254 {denBlaauwen:2017dq}. Second, after approximately 20% of the cell division cycle the
255 remaining proteins assemble subsequently at the division site. To obtain more details on PBP4
256 localization in relation to other cell division proteins, MC4100 cells were grown to steady state
257 in minimal glucose medium at 28°C. The cells were immunolabeled with antibodies against

258 PBP4, FtsZ (early localizing), or FtsN) late localizing). PBP4 localized strongly at midcell and
259 hardly in the lateral cell wall (Fig. 6). To determine whether PBP4 belongs to the early or late
260 divisome localizing proteins, we analyzed the timing of its midcell localization. To this end, we
261 plotted the extra fluorescence (FCPlus) present at midcell in comparison to the amount of
262 fluorescence in the rest of the cell (Fig. 6). PBP4 localization coincided with that of FtsZ,
263 indicating that PBP4 localizes relatively early.

264 **Midcell localization of PBP4 depends on FtsE**. To investigate if PBP4 localization is
265 dependent on the presence of the Z-ring or the later localizing division associated proteins
266 we localized PBP4 in various division defective strains. First, the localization of PBP4 was
267 assessed in a strain that expressed Tre1 that ADP-ribosylates FtsZ at R174, which renders it
268 unable to participate in protofilament formation [75,76]. The inactive E415Q variant of Tre1
269 was used as negative control. PBP4 was unable to localize in cells with insufficient FtsZ
270 protofilaments to form division Z-rings (Fig. 7A), whereas it localized as in WT cells in the
271 presence of the TreE415Q variant, proving that a Z-ring is needed for PBP4 localization. Next,
272 strains harboring temperature sensitive alleles of FtsE, FtsQ and PBP3 (FtsI) were grown in
273 minimal glucose medium at 28°C to an OD_{450} of 0.2, diluted 1:4 in prewarmed medium of 28°C
274 or 42°C and grown for two mass doublings before PBP4 immunolabelling. PBP4 localized in
275 filamentous cells with thermo-labile FtsQ or PBP3 indicating that these proteins are not
276 needed to recruit PBP4 (Fig. 7B). However, PBP4 localized very diffuse around potential
277 division sites in the filamentous *ftsE*(ts) cells (Fig. 7B). This suggests that a functional FtsE is
278 important for PBP4 localization. The FtsEX/EnvC complex assists in the assembly of the
279 divisome [77,78] and is essential for amidase function to cleave PG for cell separation [43]. To
280 investigate a possible link between PBP4 and this complex we further dissected the
281 localization requirement of PBP4. PBP4 localized at division sites in a Δ*envC* strain, indicating

282 that EnvC is not needed for PBP4 localization. However, PBP4 failed to localize in a Δ*ftsEX*
283 strain (Fig. 8). To verify whether FtsE and FtsX were required for PBP4 localization we
284 constructed a Δ*ftsE* strain. The *ftsE* and *fts*X genes reside in an operon and the expression of
285 *fts*X requires the *fts*E gene [79]. We therefore constructed a Δ*ftsE* strain with a weakened
286 p*Trc*99A promoter placed upstream of *fts*X to ensure sufficient expression of FtsX. The
287 resulting strain, XL36 grew with a mild filamentous phenotype in rich medium that could be
288 complemented by the expression of FtsE(wt) (Fig S9). PBP4 did not localized at septal
289 positions in the Δ*fts*E strain XL36 (Fig. 8A) but localized normally when FtsE was expressed to
290 complement this strain (Fig 8B). This suggests that FtsE and FtsX enhance the septal
291 localization of PBP4. Interestingly, PBP4 localized at division sites in a strain lacking the three
292 amidases AmiA, AmiB and AmiC (Fig. S10) and in a strain lacking essential components of the
293 Tol-Pal system, which is involved in the coordination of OM constriction and PG invagination
294 during cell division (Fig. S10).

295 To determine whether the activity of FtsE was needed for the localization of PBP4, we
296 expressed three inactive FtsE variants that had been shown to localize to midcell
297 {Arends:2009id}. The K41Q and D162A versions of FtsE cannot bind ATP and FtsE(E163A)
298 binds ATP but cannot hydrolyze it. PBP4 was able to localize at the division site in cells that
299 expressed one of these inactive variants of FtsE as the only copy (Fig. 8B) showing that the
300 activity of FtsE is not required for the localization of PBP4.

301 **PBP4 affects the timing of the divisome assembly.** To measure the timing of divisome
302 in various strain backgrounds, we grew Δ*dacB* cells carrying either an empty plasmid or
303 plasmids constitutively expressing PBP4 or PBP4 versions to steady state in minimal glucose
304 medium at 28°C. Cells were fixed, divided into three aliquots and labeled with antibodies
305 against FtsZ, PBP4 or FtsN. We determined the timing of the arrival of these proteins at

306 midcell by analyzing fluorescence signals of several thousands of cells [80]. In the parental
307 strain FtsZ and FtsN started to localize at midcell at about 26 % and 49%, respectively, of the
308 cell cycle age. Similarly, in the Δ*dacB* strain expressing wild-type PBP4 from plasmid FtsZ and
309 FtsN started to localize at midcell at about 28% and 49%, respectively, of the cell division cycle
310 age (Fig. 9E). Expression of inactive PBP4 versions affected the timing of the divisome
311 assembly differently. Especially the Δ*dacB* cells expressing PBP4(D155A) from plasmid
312 became slightly filamentous (Fig. 9B), assembled the divisome very early and showed a longer
313 cell division period (Fig. 9E). Next, we measured the timing of the divisome assembly in the
314 absence of PBP4 in the ΔdacB strain and in its parental BW25113. A difference was observed
315 between the two strains, which was not significant due to the large variation in the
316 localization timing of FtsZ and FtsN in both strains (Fig 9F). We inferred that BW25113 is not
317 able to reach a reproducible steady state, possibly due to a known frameshift in the *rph* gene,
318 which leads to pyrimidine starvation and hence irregular DNA replication [81]. The uracil and
319 thymine that we add as standard to the minimal medium for this strain is evidently unable to
320 fully compensate the deficiency. To solve this possible issue, the *dacB* gene was deletion from
321 the wild-type strain MC4100 and the cells were grown to steady state in minimal medium in
322 the absence of an antibiotic. The results reproduced the difference between the Δ*dacB* and
323 wild-type strains but now with a significance of P = 0.0001 (Fig. 9F). No significant difference
324 between the Δ*dacB* and its parental in other parameters that could account for a change in
325 cell cycle such as mass doubling time, cell length, diameter or the percentage of constricting
326 cells was detected (Table S1). However, FtsZ started to localize (t_0) 8 min earlier in the Δ*dacB*
327 strain and reached 50% of its maximum intensity ($t_{1/2}$) 9 min earlier compared to the parental
328 strain. FtsN localized 8.4 min (t_0) and 5.7 min ($t_{1/2}$) earlier (see for an explanation of t_0 and
329 $t_{1/2}$ Fig. 9D). These results show that PBP4 profoundly affects the timing of divisome assembly.

330

331 **DISCUSSION**

332 *E. coli* contains a large number of seemingly redundant PG hydrolases, which possibly
333 fine tune peptidoglycan biogenesis and remodelling in response to environmental parameters.
334 Apart from their enzymatic activities, little is known about the actual function of most PG
335 hydrolases. Here we report that the DD-endopeptidase PBP4 localizes at midcell during septal
336 PG synthesis in *E. coli* and is important for the timing of the assembly of the division machinery.

337 **PBP4 localises at midcell during cell division in an FtsEX dependent manner.** PBP4
338 localizes predominantly at midcell during cell division in an FtsEX dependent manner. Inactive
339 PBP4 variants were able to localize at midcell indicating that substrate hydrolysis is not a
340 requirement for localization. However, a version of PBP4 lacking the non-catalytic domain 3
341 (PBP4ΔD3), which is required for activity but not β-lactam binding, did not localize to mid-cell.
342 From these results we infer that PBP4 localizes to midcell either by recognizing its substrate
343 (without the need to hydrolyse it) and/or by protein-protein interactions. PBP4 molecules
344 appear to arrive early and concomitantly with the assemblage of the proto-ring and may
345 associate to preseptal PG synthesis, which is consistent with our observation that PBP4 affects
346 the timing of divisome assembly.

347 **PBP4 might be involved in preseptal PG synthesis.** PBP4 interacts with NlpI, PBP1A
348 and LpoA and these proteins are able to form a ternary complex ([3] and (Fig. 4). PBP4ΔD3
349 interacted with PBP1A and LpoA but not with NlpI, confirming differential PBP4 binding sites
350 of PBP1A, LpoA and NlpI. The interaction with PBP1A and/or LpoA may contribute to the
351 recruitment of PBP4 at midcell, as the amount of PBP4 at midcell was slightly reduced in
352 Δ*mrcA* and Δ*lpoA* strains. PBP1A and its partner LpoA are involved in preseptal PG synthesis
353 [33,80]. Although somewhat weaker, PBP4 still localizes at putative division sites in cell

354 filaments generated with aztreonam that have lost septal synthesis but not preseptal
355 synthesis activity. Possibly, some PBP4 enriches at preseptal PG synthesis sites together with
356 PBP1A/LpoA, which localize through the interaction of PBP1A with ZipA [33], and preseptal
357 PG synthesis provides substrates for PBP4. The interaction between NlpI and PBP4 could
358 function to sequester PBP4 in the lateral wall to prevent its interaction with potential
359 substrate (Fig. 10).

360 **Why does the loss of PBP4 affects the timing of divisome assembly?** The absence of
361 PBP4 interferes with the timing of the divisome assembly. In most bacteria studied thus far,
362 the Z-ring with its associated early division proteins localizes first to prepare the future cell
363 division site, perhaps by generating the border between the side wall and the future septum
364 [33,68,82]. After a time-delay, the proteins that synthesize the bulk of the septal PG arrive
365 and septation starts [48–50]. In the absence of PBP4, the assembly of the divisome starts
366 earlier in the cell cycle and it takes more time. This change of divisome assembly could be
367 caused by direct or indirect effects. PBP4 could be directly needed to open the PG layer to
368 allow insertion of new septal material or to remodel the nascent PG to allow new insertions.
369 Alternatively, the absence of PBP4 might enable NlpI to bind other EPases, coordinating their
370 activity for remodelling the PG layer during septation. However, the robust localization of
371 PBP4 at midcell suggests a direct function for PBP4 in cleavage of existing glycan crosslinks to
372 allow the insertion of new material. Since deletion of PBP4 does not have dramatic effects,
373 another endopeptidase must be involved as well or be able to replace PBP4 to a large extend.
374 We hypothesise that during elongation sufficient PBP4 molecules are retained by NlpI in the
375 lateral wall above the PG layer to avoid promiscuous PBP4 activity (Fig. 10). This is consistent
376 with the observations that the absence of NlpI resulted in a reduced amount of PBP4 present
377 in the cells (Fig. S6 and [3]). NlpI is not enhanced at midcell [3] and therefore we do not

378 anticipate a role for NlpI in the retention of PBP4 at midcell. PBP4 might be initially recruited
379 to midcell through interactions with PBP1A and LpoA, and the FtsEX-EnvC complex, likely
380 directing PBP4's activity already to preseptal sites (Fig. 10). Once septal peptidoglycan
381 synthesis starts by the mature divisome, more substrate should become available for PBP4
382 facilitating its accumulation at midcell, which we observed in the immunolocalization
383 experiments. Hence, PBP4 could initially remove crosslinks to help AmiA and AmiB to
384 generate denuded glycan strands. These would facilitate the accumulation of FtsN, which is
385 required to initiate septal PG synthesis. Alternatively, PBP4 could simply remove old glycan
386 strands during preseptal PG synthesis. Because of its impact on the timing of the divisome
387 assembly, the first option seems to be more likely. Whether the function of PBP4 remains the
388 same during septation will need further investigation.
389

390 **MATERIALS AND METHODS**
391
392 **Culturing conditions.** *E. coli* K12 cells were grown to steady state [80] in glucose minimal
393 medium containing 6.33 g of $K_2HPO_4.3H_2O$, 2.95 g of KH_2PO_4, 1.05 g of $(NH_4)_2$, 0.10 g of
394 $MgSO_4.7\ H_2O$, 0.28 mg of $FeSO_4.7\ H_2O$, 7.1 mg of $Ca(NO_3)_2.4\ H_2O$, 4 mg of thiamine and 4 g of
395 glucose per L. For strain MC4100 and its derivatives 50 µg lysine (Gb1) and for BW25114 and
396 MG1655 derivatives 2 µg uracil, 20 µg thymidine, 50 µg arginine and glutamine (Gb4) per liter
397 pH 7.0 at 28°C or 37°C were added. Absorbance was measured at 450 nm with a 300-T-1
398 spectrophotometer (Gilford Instrument Laboratories Inc.). Alternatively, cells were grown in
399 TY (5g yeast extract, 10 g bacto trypton and 85 mM NaCl, pH 7.0), or LB, which is TY with 170
400 mM NaCl and absorbance was measured at 600 nm.
401 **Strain construction.** Strain XL35, the FtsE partial deletion strain, was constructed as
402 follows: Primers priXL221 and priXL222 were used to amplify the upstream homologous

403 sequences (*UHS*) from the *ftsE* start codon, and primers priXL223 and priXL224 were used to
404 amplify the downstream homologous sequence after the FtsE 151th amino acid (the potential
405 promoter of *ftsX*), from the MC4100 genome. Primers priXL51 and priXL54 were used to
406 amplify the kanamycin resistance cassette from plasmid pKD4 [83]. The amplified overlap PCR
407 product (*UHS-FRT-KAN-FRT-DHS*) with primers priXL221 and priXL224 was used to construct
408 the recombinant strain XL34 in which the first 150 amino acids encoding sequence of *ftsE* was
409 deleted [83]. Subsequently, the kanamycin selection cassette was removed with plasmid
410 pCP20 [83] yielding XL35.

411 Strain XL36, the *ftsE* clean deletion strain, was constructed similarly as XL35. Primers
412 priXL221 and priXL222 were used to amplify the upstream homologous sequences from the
413 *ftsE* start codon, and primers priXL225 and priXL226 were used to amplify the downstream
414 homologous sequences after the *ftsE* stop codon, from the MC4100 genome. In order to
415 restore the FtsX expression, a *pTrc99Adown* promoter [84] was amplified from plasmid
416 pSAV057 [85] with primers priXL77 and priXL227 and a chloramphenicol selection cassette
417 was amplified from plasmid pKD3 with primers priXL52 and priXL54. The amplified overlap
418 PCR product (*UHS-FRT-CAM-FRT-DHS*) with primers priXL221 and priXL226 was used to
419 construct the recombinant strain XL33 in which the entire *ftsE* coding sequence was deleted
420 and FtsX was expressed from the chromosomally encoded p*Trc99Adown* promoter.
421 Subsequently, the kanamycin selection cassette was removed with plasmid pCP20 yielding
422 XL36 (Table 1).

423 **Plasmid construction**. The *ftsE* gene was amplified from the chromosome of LMC500
424 [86] using the forward primer priXL187 and the reverse primer priXL188, and sequenced to
425 characterize the mutation. The wild-type *ftsE* gene was cloned into pSAV057, p15A origin and
426 Cam^{R} [85] to produce the plasmid pXL135. *FtsE* was expressed under the control of the

427 p*Tcr*99A down promoter. QuickChange site directed mutagenesis (Agilent technologies, Santa
428 Clara, CA) and Gibson assembly [87] approaches were applied afterwards to construct the
429 inactive *ftsE* mutant plasmids pXL137, pXL138 and pXL139, using the primers listed in Table 2.
430 To construct the PBP4 expression plasmids, the wild-type *dacB* gene was firstly
431 amplified from the *E. coli MG1655* genome using primers priXL244 and priXL245, and
432 subsequently cloned into plasmid pSAV057 and pSAV057-dsba^{ss}-mCherry-PBP5 (pNM010 [20])
433 with *EcoRI* and *HindIII*, to generate the PBP4 plasmids without and with mCherry fusion.
434 Similarly, QuickChange site directed mutagenesis and Gibson assembly approaches were
435 applied afterwards to construct the inactive *dacB* mutant plasmids from these two wild-type
436 plasmids, using the primers listed in Table 2. Tre1 and Tre1E415Q were expressed from the
437 arabinose inducible promoter of pBAD18 as described [75].
438 **Immunolabeling**. After reaching steady state for minimal glucose grown cells or the
439 desired OD for rich medium grown cells, the cells were fixed for 15 min by addition of a
440 mixture of formaldehyde (f. c. 2.8%) and glutaraldehyde (f. c. 0.04%) to the cultures in the
441 shaking water bath and immunolabeled as described [88] with Rabbit polyclonal antibodies
442 against PBP4, NlpI [3] preabsorbed against *ΔdacB* or *ΔnlpI*, strains, respectively, or against
443 FtsZ or FtsN [48]. As secondary antibody, donkey anti-rabbit conjugated to Cy3 or to Alexa488
444 (Jackson Immunochemistry, USA) diluted 1:300 in blocking buffer (0.5% (wt/vol) blocking
445 reagents (Boehringer, Mannheim, Germany) in PBS) was used, and the samples were
446 incubated for 30 minutes at 37°C. For immunolocalization, cells were immobilized on 1%
447 agarose in PBS slabs coated object glasses as described [76] and photographed with an Orca
448 Flash 4.0 (Hamamatsu, Japan) CCD camera mounted on an Olympus BX-60 (Japan)
449 fluorescence microscope through a 100x/*N.A*. 1.35 oil objective. Images were taken using the
450 program ImageJ with MicroManager (https://www.micro-manager.org).

451 SIM images were obtained with a Nikon Ti Eclipse microscope (Japan) and captured
452 using a Hamamatsu Orca-Flash 4.0 LT camera. Phase contrast images were acquired with a
453 Plan APO 100x/1.45 Ph3 oil objective. SIM images were obtained with a SR APO TIRF
454 100x/1.49 oil objective, using 3D-SIM illumination with a 561nm laser, and were
455 reconstructed with Nikon-SIM software using the values 0.20-0.25-0.20 for the parameters
456 Illumination Modulation Contrast (IMC), High Resolution Noise suppression (HNS) and Out of
457 focus Blur Suppression (OBS), respectively.

458 **Image analysis.** Phase contrast and fluorescence images were combined into
459 hyperstacks using ImageJ (http://imagej.nih.gov/ij/) and these were linked to the project file
460 of Coli-Inspector running in combination with the plugin ObjectJ
461 (https://sils.fnwi.uva.nl/bcb/objectj/). The images were scaled to 15.28 pixel per μm. The
462 fluorescence background has been subtracted using the modal values from the fluorescence
463 images before analysis. Slight misalignment of fluorescence with respect to the cell contours
464 as found in phase contrast was corrected using Fast-Fourier techniques as described [80].
465 Data analysis was performed as described [80]. In brief, midcell was defined as the central
466 part of the cell comprising 0.8 μm of the axis. From either cell part, midcell and remaining cell,
467 the volume, the integrated fluorescence, and thus the concentration of fluorophores was
468 calculated. The difference of the two concentrations is multiplied with the volume of midcell.
469 It yields FCPlus (surplus of fluorescence) at midcell. For age calculation, all cell lengths are
470 sorted in ascending order. Then the equation

471 age = ln(1 - 0.5 * rank / (nCells - 1)) / ln(0.5)

472 is used, where *rank* is a cell's index in the sorted array, *nCells* is the total number of cells, and
473 *age* is the cell's age expressed in the range 0 .. 1.

474 **Ni^{2+}-NTA pulldown assays**. Nickel-Nitrilotriacetic acid (Ni-NTA) beads (100µl) were
475 pre-equilibrated with dH_2O and binding buffer (10 mM HEPES/NaOH, 10 mM $MgCl_2$, 150 mM
476 NaCl, 0.05% Triton X-100, pH 7.5) by centrifugation at 4000 × *g*, 4 min at 4°C, and then
477 incubated with proteins of interest. Equimolar amounts (1-2 µM) of His_6-tagged and untagged
478 proteins were incubated alone (control) and in combination, for 10 min at 4°C in a 200 µl
479 reaction volume, containing 10 mM binding buffer. An aliquot of this mixture is taken as an
480 'applied' sample. The protein samples were then added to pre-equilibrated Ni-NTA beads and
481 incubated overnight on a spinning plate at 4°C with 1.3 ml of binding buffer.

482 Beads were centrifuged at 4000 × *g*, 4 min, 4°C and washed a further 4-6 times with 1
483 ml of washing buffer (binding buffer with 30 mM Imidazole) before re-suspending in 250 µl
484 washing buffer and transferring beads to Proteus spin columns (Generon), centrifuging as
485 described above. Bound proteins were eluted by the addition of 50 µl of SDS-PAGE loading
486 buffer and boiling at 100°C for 5 min. Spin columns were centrifuged a final time at 1500 × *g*,
487 5 min, RT, to collect 'eluted' protein before separation by SDS-PAGE. Eluted samples were run
488 alongside applied samples for comparison.

489 **Microscale thermophoresis.** Microscale thermophoresis (MST) is an immobilisation-
490 free method which allows the detection of biomolecular interactions in solution. This
491 technique is based on the specific directed movement of a protein along a heat gradient
492 (thermophoresis), an observation first reported by Carl Ludwig in 1856 [89]. The
493 thermophoresis of a protein changes upon ligand binding due to one or more changes to size,
494 charge and/or hydration shell. In MST, a localized heat gradient is initiated by an IR-laser
495 (wavelength 1470 nm). A protein of interest is fluorescently labelled and the change in its
496 thermophoretic mobility, in the presence of an unlabelled ligand, is measured and expressed
497 as a change in the normalised fluorescence (FNorm).

498 Proteins of interest (10-20 μM) were fluorescently labelled with an amine
499 reactive dye (NT-647- N-hydroxysuccinimide (NHS)), cysteine reactive dye (NT-647 maleimide)
500 or a histidine reactive dye (NT-647-Tris-NTA), according to manufacturer's instructions
501 (Nanotemper). Fluorescently labelled proteins were diluted to an appropriate concentration
502 and a fixed concentration was titrated against a two-fold serial dilution of unlabelled ligand,
503 across 16 samples, in MST running buffer (25 mM HEPES/NaOH, 150 mM NaCl, 0.05% Triton
504 X-100, pH 7.5).

505 MST measurements were carried out as described in [90], using standard or premium
506 capillaries on a Monolith NT.115^{TM} MST machine (Nanotemper). Binding curves and Kinetic
507 parameters were plotted and estimated using manufacturer provided software (NT Analysis
508 1.5.41 and MO. Affinity Analysis (x64)). Capillary scans were carried out prior to all
509 measurements to check for consistent fluorescence counts, confirming that any subsequent
510 change in fluorescence was due to ligand binding and not due to inaccurate pipetting or
511 adsorption and dilution effects.

512 **SDS-denaturation (SD) test.** In instances where capillary scans showed a ligand
513 concentration dependant change in raw fluorescence, we investigated whether this was a
514 property of the binding interaction by carrying out an SD-test.

515 Samples (10 μL) with the highest and lowest concentration of unlabelled ligand were
516 centrifuged 10 000 × *g,* 5 min, RT and mixed 1:1 volume ratio with SD-test buffer (40 mM DTT,
517 4% SDS). Mixtures were boiled at 100 °C for 10 min, to abolish ligand binding, before being
518 spun down and subjected to another capillary scan. If the fluorescence between samples that
519 contained the highest and lowest concentration of ligand, after SDS treatment, were now
520 back to ± 10% of each other, the initial observations were a property of ligand binding, and a
521 binding curve was plotted from the raw fluorescence data. If the ligand concentration

522 dependent change in fluorescence was still observed, then this indicated that the
523 fluorescently labelled protein was aggregated, and assay and buffer conditions were
524 optimised accordingly

525 ***In vivo* cross-linking / co-immunoprecipitation assays.** Method is described in, and
526 adapted from [91]. An overnight culture of *E. coli* BW25113 cells and an appropriate mutant
527 strain was used to inoculate 150 ml of Lennox LB (Fisher Scientific) and was cultivated to an
528 OD_{578} of 0.5-0.6 at 37°C before harvesting by centrifugation (4500 × g, 4°C, 25 min). Cells were
529 resuspended in 6 ml of CL buffer 1 (50 mM NaH_2PO_4, 20% sucrose, pH 7.4). The amine reactive
530 cross-linker, DTSSP (3,3'-dithiobis (sulfosuccinimidylpropionate) (ThermoFisher), was freshly
531 dissolved (20 mg/ml in dH_2O) and added to the isolated cell suspension and incubated at 4°C
532 with agitation for 1 h. Cross-linked cells were then harvested by centrifugation (4500 × g, 4°C,
533 25 min) and resuspended in 6 ml CL buffer 2 (100 mM Tris/HCl, 10 mM $MgCl_2$, 1 M NaCl, pH
534 7.5). DNase, protease inhibitor cocktail and phenylmethylsulfonly fluoride were added prior
535 to sonication at low levels before ultracentrifugation of the lysate (140,000 × g, 4°C, 1 h). The
536 membrane pellet was resuspended in 2.5 ml of CL buffer 3 (25 mM Tris/HCl, 10 mM $MgCl_2$, 1
537 M NaCl, 1% Triton X-100, 20% glycerol, pH 7.5) and the solubilised membrane extracted o/n
538 with stirring at 4°C.

539 Samples were ultracentrifuged (140,000 × *g*, 4°C, 1 h) to remove debris, before
540 removing 2 × 1.2 ml of each supernatant to be subsequently diluted with 0.6 ml of CL buffer
541 4 (75 mM Tris/HCl, 10 mM $MgCl_2$, 1 M NaCl, pH 7.5). One sample was incubated with an
542 optimised concentration of specific antibody with the other used as a negative control. Both
543 samples were incubated at 4°C with agitation for 5 h. For the isolation of antibodies, and thus
544 cross-linked interaction partners, 100 µl of protein G-coupled agarose bead resin (Roche)

545 were washed (2 × CL buffer 4, 2 × CL wash buffer [2:1 CL buffer 3 and CL buffer 4]) and added
546 to each sample, and incubated o/n at 4°C with agitation.

547 Samples were centrifuged and the supernatant retained before washing the beads 10
548 × 1 ml with CL wash buffer. After the final wash, beads were resuspended in 250 µl CL wash
549 buffer and transferred to 2 ml spin dry columns and centrifuged to isolate the beads. These
550 were then resuspended in 50 µl of fresh SDS-loading buffer and boiled to elute bound proteins,
551 and reverse cross-linkage, and were collected by centrifugation (10,000 × *g*, RT, 5 min).
552 Supernatant and elution samples were resolved by SDS-PAGE and transferred to a
553 nitrocellulose membrane by Western blotting to detect for specific interaction partners using
554 purified antibodies. The secondary antibody used here is Trueblot Anti-Rabbit IgG-HRP
555 specific for native antibodies.

556 **Peptidoglycan digestion assays**. To test for hydrolase activity on PG, 10 µl of sacculi
557 isolated from strains of interest (usually *E. coli* strains MC1061, BW25113 or D456) were
558 incubated with 1-10 µM of respective enzymes, 37°C for between 1 h and overnight, as
559 indicated for respective proteins. The standard reaction conditions were 10 mM HEPES/NaOH,
560 10 mM $MgCl_2$, 150 mM NaCl, 0.05% Triton X-100, pH 7.5, in 100 µl reaction volume. Following
561 incubation, samples were boiled at 100°C, 10 min, to terminate reactions before digesting
562 remaining PG overnight at 37°C, with 1 µM cellosyl. The samples were centrifuged at 10,000
563 × *g* for 5 min, RT, to obtain digested muropeptide products in the supernatant.

564 To test for activity against soluble muropeptides; first, 100 µl of intact sacculi were
565 incubated overnight at 37°C with 1 µM cellosyl and cellosyl digestion buffer (20 mM $NaPO_4$,
566 pH 4.8). Next, samples were boiled at 100 °C, 10 min, before centrifugation at 10,000 × *g* for
567 5 min, RT, to obtain the soluble muropeptides in the supernatant [92]. Ten µl of the
568 supernatant was then used as muropeptide substrate for incubating with enzymes of interest,

569 for the appropriate incubation time, at 37°C. Reactions were then terminated by boiling at
570 100°C for 10 min.

571 After digestion of respective substrates, products were reduced with $NaBH_4$, adjusted
572 to pH 4-5 and separated for analysis by reversed-phase HPLC as described below in HPLC
573 analysis.

574 **Reduction of muropeptides with sodium borohydride.** PG digestion samples were
575 transferred to 2 ml vials following centrifugation. Muropeptides were reduced in a 1:1 volume
576 ratio of sodium borohydride buffer (0.5 M sodium borate, pH 9.0) and a small spatula of
577 sodium borohydride pellets, centrifuging at 3000 × *g,* 30 min, RT as described in [92]. The
578 samples were adjusted to pH 4-5 using HPLC grade phosphoric acid before separation and
579 analysis by reversed-phase HPLC.

580 **Reversed-phase HPLC analysis of muropeptides.** Following the protocol of [92],
581 reduced muropeptides were separated for analysis on reversed-phase HPLC systems with a
582 Prontosil 120-3-C18-AQ 3 µm reversed-phase HPLC column (Bischoff). A linear gradient of
583 solvent A (50 mM sodium phosphate, pH 4.31 supplemented with 0.2% NaN_3) to 100 %
584 solvent B (75 mM sodium phosphate, pH 4.95, 15% methanol) over 90 or 180 min was used
585 to separate muropeptides at 52°C. Unlabelled muropeptides were detected at UV absorbance
586 205 nm. In assays where ^{14}C-radiolabelled muropeptides were used, detection was achieved
587 by flowing scintillation cocktail along with standard buffers to give a radioisotope scintillation
588 count (radioactivity CPM). Muropeptide profiles were recorded and analysed using Laura
589 V4.2.11.129 (LabLogic Systems Ltd.).

590 **Spectrophotometric D-alanine release assay (DD-carboxypeptidase assay).** This
591 protocol was adapted from [62]. The carboxypeptidase (CPase) activity of PG hydrolases
592 results in the release of the terminal D-Ala residue from the pentapeptide stem of PG

593 precursors. Using UDP-Mur*N*Ac pentapeptide as a substrate, and in this case PBP4, it was
594 possible to spectrophotometrically measure the release of D-Ala.

595 Each reaction sample consisted of 200 µl of CPase buffer (50 mM HEPES/NaOH, 10
596 mM $MgCl_2$, pH 7.6), 3 units of D-amino acid oxidase (Sigma), 6 units of horseradish peroxidase
597 (HRP) (Sigma), Amplex Red (Sigma), and an optimised concentration of protein.

598 All constituents of the reaction were added and mixed directly in a quartz cuvette
599 (Hellma, 10 mM light path, 15 mM centre), before the addition, and brief mixing by pipette,
600 of purified UDP-Mur*N*Ac pentapeptide (BACWAN, Warwick University) to begin the reaction.
601 The released D-Ala residues from the CPase activity of PBP4 are oxidatively deaminated by
602 the action of D-amino acid oxidase to produce pyruvate and hydrogen peroxide (H_2O_2). The
603 released H_2O_2 is reduced to H_2O by HRP using Amplex Red as an electron donor. Oxidised
604 Amplex Red produces resorufin, which has an intense pink colour and the production of which
605 was measured spectrophotometrically using a Cary 100 Bio UV-visible spectrophotometer
606 (wavelength 555 nm). The change in absorption over 10 min was measured and analysed
607 using the complementing software.

608 **Circular dichroism.** Proteins were dialysed overnight against 10 mM $NaPO_4$, pH 7.5
609 and concentrated/diluted to 0.4 mg/ml. CD measurements were taken using a Jasco J-810
610 spectropolarimeter using a wavelength range of 180-250 nm. The average of 10 runs was
611 taken for each protein with a buffer control subtraction. For a direct comparison, correcting
612 for the differing amino acid sequences, the collected data were converted to molecular CD
613 and plotted against wavelength (nm). The resulting CD spectra are compared in Fig. S4 and
614 show that PBP4 lacking domain 3 is folded, consisting of both α-helices (~190, 208 and 222
615 nm) and β-sheets (~210 nm).

616 **Analytical ultracentrifugation.** Purified PBP4 and PBP4ΔD3 were dialyzed over night
617 against 25 mM HEPES/NaOH, 150 mM NaCl, pH 7.5, in preparation for AUC experiments. AUC
618 sedimentation velocity (SV) experiments were carried out in a Beckman Coulter (Palo Alto,
619 CA, USA) ProteomeLab XL-I analytical ultracentrifuge using absorbance at 280 nm and
620 interference detection. The AUC runs were executed at the rotation speed of 45,000 rpm and
621 the temperature of 20°C using an 8-hole AnTi50 rotor and double-sector aluminium-Epon
622 centerpieces. The sample volume was 400 µl and the sample concentrations ranged between
623 approximately 0.25 and 1.4 mg/ml. The partial specific volumes ($\bar{v}$) of the proteins were
624 calculated from their amino acid sequence, using the program SEDNTERP [93]. Sedimentation
625 velocity boundaries were analyzed using the size-distribution c(s) model implemented in the
626 program SEDFIT http://www.analyticalultracentrifugation.com [94]. The experimental values
627 of the sedimentation coefficient were converted to the standard conditions (s20,w), which is
628 the value of sedimentation coefficient in water at 20°C. The size-distribution peaks were
629 integrated to obtain the weight-averaged values for sedimentation coefficient and molecular
630 mass.

631 The atomic coordinates from the published high-resolution structure of [60] (pdb
632 accession code 2EX2) were used to calculate the sedimentation coefficient values for the
633 monomeric and dimeric forms of PBP4 /PBP4ΔD3 using the program SoMo [95]. PBP4
634 /PBP4ΔD3 crystallographic dimer was built using program PyMol (https://pymol.org/2/).

635 **PG binding assay.** To assay for interactions of respective proteins with purified PG, we
636 used a PG binding protocol as described in [96]. Briefly, ~100 µg purified PG was pelleted by
637 centrifugation (10,000 × *g,* 10 min, 4°C) and resuspended in binding buffer (10 mM
638 Tris/Maleate, 10 mM $MgCl_2$, 50 mM NaCl, pH 6.8). PG was incubated with 10 µg of desired
639 protein before incubating on ice for 30 min and centrifuging at 10,000 × *g,* 10 min, 4°C. An

640 aliquot of the supernatant (S) was taken for SDS-PAGE. The pelleted PG was washed with 200
641 µl binding buffer by centrifugation as before and the wash supernatant was taken as sample
642 W for SDS-PAGE. The pelleted PG was then resuspended in 100 µl of 2% SDS and incubated
643 for 1 h on a stirring plate, 4°C. Mixtures were centrifuged a final time at 10,000 × *g,* 10 min,
644 4°C, with the supernatant, now containing any initially bound protein, taken as the pellet
645 sample (P). A negative control sample with no PG was assayed in parallel to determine that
646 binding of protein was specific. Samples, along with corresponding controls, were analysed
647 by SDS-PAGE and visualised by Coomassie staining. Presence of protein band in pellet sample
648 (P) indicated binding to PG, whilst presence in supernatant sample (S) indicated no binding.
649 **Bocillin binding assay.** A fluorescent-bocillin binding assay was used to determine
650 whether a PBP was purified with a correctly folded active site. Bocillin FL is a commercially
651 available dye-β-lactam conjugate, synthesised from penicillin V and BODIPY (Molecular
652 Probes, In., Eugene, Oreg.). Ten µg of purified PBP was incubated for 10 min at 37°C, with 20
653 ng of Bocillin FL in a 50 µl volume with 10 mM HEPES/NaOH, 10 mM $MgCl_2$, pH 7.5. A negative
654 control sample was pre-incubated with 1 mM ampicillin for 30 min, 37°C, to block the PBP
655 active site, prior to incubation with Bocillin FL. After incubation, samples were boiled at 100
656 °C for 10 min with 40 µl of SDS-PAGE loading buffer and resolved by SDS-PAGE. Fluorescent
657 signal was observed using Typhoon Fluorescence-imager (Excitation; 488 nm, emission; 520
658 nm, BP20 PMT 400-600 V), followed by visualisation of gels by Coomassie staining. Proteins
659 incubated with ampicillin should have no detectable binding of Bocillin FL. For whole cells, a
660 culture was grown in 5 mL TY and induced with 10 µM IPTG for 3 mass doublings to an OD_{600}
661 of 0.5 and the cells were pelleted and washed once with PBS (8 g NaCl, 1.8 g Na_2HPO_4, 0.24 g
662 KH_2PO_4 per liter, adjusted to pH 7.4) at 4°C and resuspended in 100 µl PBS with 5µg/ml Bocilin
663 FL and incubated for 20 min at RT. To remove the excess Bocillin FL, the samples were pelleted

664 and resuspended in 100 μl PBS with cOmplete™ Mini Protease Inhibitor Cocktail (Sigma) and
665 2 U DNAse I (NEB). Then sonicated on ice for 10 sec and boiled 15' at 99°C after adding 25 μL
666 of SDS-PAGE 5x loading buffer and resolved by SDS-PAGE. Fluorescent signal was observed
667 using a home-made imager for Midori green, followed by visualisation of gels by Coomassie
668 staining.

669 ***In vitro* PG synthesis assay with radiolabelled lipid II.** The assay was published by
670 Bertsche et al., [97]. Lipid II (1.2 nmol, 11,000 dpm) was vacuum dried and dissolved in 5 µl of
671 methanol. The reaction was performed in a total volume of 50 µl in 25 mM Tris/HCl, 10 mM
672 $MgCl_2$, 100 mM NaCl, 0.05% Triton X-100, pH 7.5 (buffer B), with 0.5 µM PBP1A, 1 µM LpoA,
673 1 µM PBP4(S62A), 2 µM NlpI. The reaction was performed for 1 h at 30°C. The pH of the
674 samples was adjusted to 4.8 prior to boiling for 5 min followed by a digestion with 50 g/ml
675 cellosyl for 1 h at 37°C and boiling for 5 min.

676

677 **ACKNOWLEDGEMENTS**

678 We thank David Roper and Smita Chauhan (University of Warwick) for help with the
679 carboxypeptidase assay, Helen Waller (Newcastle University) for help with circular dichroism
680 methodology, Lisa Atkinson and Daniela Vollmer (Newcastle University) for preparation of PG
681 sacculi, and Thomas van Wingen for with help the Tre1 assay. We thank See-Yeun Ting for the
682 plasmids expressing Tre1 and Tre1E415Q (University of Washington School of Medicine,
683 Seattle, USA). The work was supported by funding from the Wellcome Trust (101824/Z/13/Z),
684 to WV). X.L. was supported by the China Scholarship Council fellowship (File
685 No.201406220123).

686 J.V., A.L., H.C.L.Y, X.L., X.L., A.S.S., and M.B did most experiments. A.T., M.B., V.W., and T.dB.

687 designed most experiments. M.B, W.V and T.dB analyzed the data and wrote the manuscript.

688 All authors critically read the manuscript and provided feedback.

689 **References**

690 1. Vollmer W, Blanot D, Pedro MAD. Peptidoglycan structure and architecture. FEMS microbiol. revs. 2008;32:
691 149–167. doi:10.1111/j.1574-6976.2007.00094.x

692 2. Egan AJF, Errington J, Vollmer W. Regulation of peptidoglycan synthesis and remodelling. Nat. Rev. Microbiol.
693 2020;18: 446–460. doi:10.1038/s41579-020-0366-3

694 3. Banzhaf M, Yau HCL, Verheul J, Lodge A, Kritikos G, Mateus A, et al. Outer membrane lipoprotein NlpI scaffolds
695 peptidoglycan hydrolases within multi-enzyme complexes in Escherichia coli. The EMBO Journal. 2020;
696 e102246. doi:10.15252/embj.2019102246

697 4. Gray AN, Egan AJF, Veer ILV, Verheul J, Colavin A, Koumoutsi A, et al. Coordination of peptidoglycan synthesis
698 and outer membrane constriction during *Escherichia coli* cell division. Storz G, editor. eLife. 2015;4:
699 e07118. doi:10.7554/elife.07118

700 5. Bertsche U, Kast T, Wolf B, Fraipont C, Aarsman MEG, Kannenberg K, et al. Interaction between two murein
701 (peptidoglycan) synthases, PBP3 and PBP1B, in Escherichia coli. Molecular Microbiology. 2006;61: 675–
702 690. doi:10.1111/j.1365-2958.2006.05280.x

703 6. Born P, Breukink E, Vollmer W. In vitro synthesis of cross-linked murein and its attachment to sacculi by PBP1A
704 from *Escherichia coli*. J. Biol. Chem. 2006;281: 26985–26993. doi:10.1074/jbc.m604083200

705 7. Egan AJF, Biboy J, Veer I van't, Breukink E, Vollmer W. Activities and regulation of peptidoglycan synthases.
706 Philosophical transactions of the R.Soc. London Series B, Biolog. Sci. 2015;370.
707 doi:10.1098/rstb.2015.0031

708 8. Pazos M, Vollmer W. Regulation and function of class A Penicillin-binding proteins. Curr. Opin. Microbiol.
709 2021;60: 80–87. doi:10.1016/j.mib.2021.01.008

710 9. Rohs PDA, Buss J, Sim SI, Squyres GR, Srisuknimit V, Smith M, et al. A central role for PBP2 in the activation of
711 peptidoglycan polymerization by the bacterial cell elongation machinery. PLoS Genetics. 2018;14:
712 e1007726. doi:10.1371/journal.pgen.1007726

713 10. Meeske AJ, Riley EP, Robins WP, Uehara T, Mekalanos JJ, Kahne D, et al. SEDS proteins are a widespread
714 family of bacterial cell wall polymerases. Nature. 2016;537: 634–638. doi:10.1038/nature19331

715 11. Taguchi A, Welsh MA, Marmont LS, Lee W, Sjodt M, Kruse AC, et al. FtsW is a peptidoglycan polymerase that
716 is functional only in complex with its cognate penicillin-binding protein. Nat. Microbiol. 2019;4: 587–594.
717 doi:10.1038/s41564-018-0345-x

718 12. Ploeg R van der, Verheul J, Vischer NOE, Alexeeva S, Hoogendoorn E, Postma M, et al. Colocalization and
719 interaction between elongasome and divisome during a preparative cell division phase in *Escherichia*
720 *coli.* Mol. Microbiol. 2013;87: 1074–1087. doi:10.1111/mmi.12150

721 13. Datta P, Dasgupta A, Singh AK, Mukherjee P, Kundu M, Basu J. Interaction between FtsW and penicillin-
722 binding protein 3 (PBP3) directs PBP3 to mid-cell, controls cell septation and mediates the formation of

723 a trimeric complex involving FtsZ, FtsW and PBP3 in mycobacteria. Mol. Microbiol. 2006;62: 1655–1673.
724 doi:10.1111/j.1365-2958.2006.05491.x

725 14. Fraipont C, Alexeeva S, Wolf B, Ploeg R van der, Schloesser M, Blaauwen T den, et al. The integral membrane
726 FtsW protein and peptidoglycan synthase PBP3 form a subcomplex in *Escherichia coli*. Microbiol.
727 2011;157: 251–259. doi:10.1099/mic.0.040071-0

728 15. Liu X, Biboy J, Consoli E, Vollmer W, Blaauwen den, T. MreC and MreD balance the interaction between the
729 elongasome proteins PBP2 and RodA. PLoS Genetics. 2020;16: e1009276.
730 doi:10.1371/journal.pgen.1009276

731 16. Pazos M, Peters K, Vollmer W. Robust peptidoglycan growth by dynamic and variable multi-protein
732 complexes. Curr. Opin. Microbiol. 2017;36: 55–61. doi:10.1016/j.mib.2017.01.006

733 17. Sarkar SK, Dutta M, Chowdhury C, Kumar A, Ghosh AS. PBP5, PBP6 and DacD play different roles in intrinsic -
734 lactam resistance of *Escherichia coli.* Microbiology (Reading, England). 2011;157: 2702–2707.
735 doi:10.1099/mic.0.046227-0

736 18. Potluri L, Karczmarek A, Verheul J, Piette A, Wilkin J-M, Werth N, et al. Septal and lateral wall localization of
737 PBP5, the major D,D-carboxypeptidase of *Escherichia coli*, requires substrate recognition and membrane
738 attachment. Mol. Microbiol. 2010;77: 300–323. doi:10.1111/j.1365-2958.2010.07205.x

739 19. Hugonnet J-E, Mengin-Lecreulx D, Monton A, Blaauwen T den, Carbonnelle E, Veckerlé C, et al. Factors
740 essential for L,D-transpeptidase-mediated peptidoglycan cross-linking and β-lactam resistance in
741 *Escherichia coli*. eLife. 2016;5: 2006. doi:10.7554/elife.19469

742 20. Meiresonne NY, Ploeg R van der, Hink MA, Blaauwen T den. Activity-Related Conformational Changes in d,d-
743 Carboxypeptidases Revealed by In Vivo Periplasmic Förster Resonance Energy Transfer Assay in
744 *Escherichia coli.* Søgaard-Andersen L, editor. mBio. 2017;8: e01089-17. doi:10.1128/mbio.01089-17

745 21. Singh SK, Saisree L, Amrutha RN, Reddy M. Three redundant murein endopeptidases catalyse an essential
746 cleavage step in peptidoglycan synthesis of *Escherichia coli* K12. Mol. Microbiol. 2012;86: 1036–1051.
747 doi:10.1111/mmi.12058

748 22. Meberg BM, Paulson AL, Priyadarshini R, Young KD. Endopeptidase penicillin-binding proteins 4 and 7 play
749 auxiliary roles in determining uniform morphology of *Escherichia coli.* J. Bacteriol. 2004;186: 8326–8336.
750 doi:10.1128/jb.186.24.8326-8336.2004

751 23. Peters K, Kannan S, Rao VA, Biboy J, Vollmer D, Erickson SW, et al. The Redundancy of Peptidoglycan
752 Carboxypeptidases Ensures Robust Cell Shape Maintenance in *Escherichia coli*. mBio. 2016;7.
753 doi:10.1128/mbio.00819-16

754 24. Peters NT, Dinh T, Bernhardt TG. A fail-safe mechanism in the septal ring assembly pathway generated by the
755 sequential recruitment of cell separation amidases and their activators. J. Bacteriol. 2011;193: 4973–
756 4983. doi:10.1128/jb.00316-11

757 25. Heidrich C, Templin MF, Ursinus A, Merdanovic M, Berger J, Schwarz H, et al. Involvement of N-
758 acetylmuramyl-L-alanine amidases in cell separation and antibiotic-induced autolysis of *Escherichia coli.*
759 Mol. Microbiol. 2001;41: 167–178.

760 26. Bernhardt TG, Boer PAJD. The Escherichia coli amidase AmiC is a periplasmic septal ring component exported
761 via the twin-arginine transport pathway. Mol. Microbiol. 2003;48: 1171–1182.

762 27. Uehara T, Parzych KR, Dinh T, Bernhardt TG. Daughter cell separation is controlled by cytokinetic ring-
763 activated cell wall hydrolysis. EMBO J. 2010;29: 1412–1422. doi:10.1038/emboj.2010.36

764 28. Straaten KE van, Dijkstra BW, Vollmer W, Thunnissen A-MWH. Crystal structure of MltA from *Escherichia coli*
765 reveals a unique lytic transglycosylase fold. J. Mol. Biol. 2005;352: 1068–1080.
766 doi:10.1016/j.jmb.2005.07.067

767 29. Heijenoort J van. Peptidoglycan hydrolases of *Escherichia coli.* Microbiol and Mol. Biol. Revs.: MMBR.
768 2011;75: 636–663. doi:10.1128/mmbr.00022-11

769 30. Yunck R, Cho H, Bernhardt TG. Identification of MltG as a potential terminase for peptidoglycan
770 polymerization in bacteria. Mol.Microbiol. 2015. doi:10.1111/mmi.13258

771 31. Addinall SG, Lutkenhaus J. FtsZ-spirals and -arcs determine the shape of the invaginating septa in some
772 mutants of *Escherichia coli*. Mol. Microbiol. 1996;22: 231–237.

773 32. Raychaudhuri D. ZipA is a MAP-Tau homolog and is essential for structural integrity of the cytokinetic FtsZ
774 ring during bacterial cell division. EMBO J. 1999;18: 2372–2383. doi:10.1093/emboj/18.9.2372

775 33. Pazos M, Peters K, Casanova M, Palacios P, VanNieuwenhze M, Breukink E, et al. Z-ring membrane anchors
776 associate with cell wall synthases to initiate bacterial cell division. Nature Commun. 2018;9: 5090–12.
777 doi:10.1038/s41467-018-07559-2

778 34. Galli E, Gerdes K. FtsZ-ZapA-ZapB Interactome of Escherichia coli. J.Bacteriol. 2012;194: 292–302.
779 doi:10.1128/jb.05821-11

780 35. Durand-Heredia JM, Yu HH, Carlo SD, Lesser CF, Janakiraman A. Identification and Characterization of ZapC, a
781 Stabilizer of the FtsZ Ring in *Escherichia coli.* J. Bacteriol. 2011;193: 1405–1413. doi:10.1128/jb.01258-10

782 36. Hale CA, Shiomi D, Liu B, Bernhardt TG, Margolin W, Niki H, et al. Identification of *Escherichia coli* ZapC
783 (YcbW) as a component of the division apparatus that binds and bundles FtsZ polymers. J. Bacteriol.
784 2011;193: 1393–1404. doi:10.1128/jb.01245-10

785 37. Roach EJ, Wroblewski C, Seidel L, Berezuk AM, Brewer D, Kimber MS, et al. Structure and mutational analyses
786 of *Escherichia coli* ZapD reveal charged residues involved in FtsZ filament bundling. DiRita VJ, editor. J.
787 Bacteriol. 2016;198: 1683–1693. doi:10.1128/jb.00969-15

788 38. Marteyn BS, Karimova G, Fenton AK, Gazi AD, West N, Touqui L, et al. ZapE is a novel cell division protein
789 interacting with FtsZ and modulating the Z-ring dynamics. mBio. 2014;5: e00022-14.
790 doi:10.1128/mbio.00022-14

791 39. Mehla J, Liechti G, Morgenstein RM, Caufield JH, Hosseinnia A, Gagarinova A, et al. ZapG (YhcB/DUF1043), a
792 novel cell division protein in gamma-proteobacteria linking the Z-ring to septal peptidoglycan synthesis.
793 J Biol Chem. 2021;296: 100700. doi:10.1016/j.jbc.2021.100700

794 40. Du S, Pichoff S, Lutkenhaus J. FtsEX acts on FtsA to regulate divisome assembly and activity. Proc. Natl Acad
795 Sci. USA. 2016;113: E5052-61. doi:10.1073/pnas.1606656113

796 41. Corbin BD, Wang Y, Beuria TK, Margolin W. Interaction between Cell Division Proteins FtsE and FtsZ. J.
797 Bacteriol. 2007;189: 3026–3035. doi:10.1128/jb.01581-06

798 42. Priyadarshini R, Popham DL, Young KD. Daughter Cell Separation by Penicillin-Binding Proteins and
799 Peptidoglycan Amidases in *Escherichia coli.* J. Bacteriol. 2006;188: 5345–5355. doi:10.1128/jb.00476-06

800 43. Yang DC, Peters NT, Parzych KR, Uehara T, Markovski M, Bernhardt TG. An ATP-binding cassette transporter-
801 like complex governs cell-wall hydrolysis at the bacterial cytokinetic ring. Proc. Natl Acad Sci. USA.
802 2011;108: E1052-60. doi:10.1073/pnas.1107780108

803 44. Yang DC, Tan K, Joachimiak A, Bernhardt TG. A conformational switch controls cell wall-remodelling enzymes
804 required for bacterial cell division. Mol. Microbiol. 2012;85: 768–781. doi:10.1111/j.1365-
805 2958.2012.08138.x

806 45. Tsang M-J, Yakhnina AA, Bernhardt TG. NlpD links cell wall remodeling and outer membrane invagination
807 during cytokinesis in Escherichia coli. PLoS Genetics. 2017;13: e1006888.
808 doi:10.1371/journal.pgen.1006888

809 46. Serrano CKG, Winkle M, Martorana AM, Biboy J, Morè N, Moynihan P, et al. ActS activates peptidoglycan
810 amidases during outer membrane stress in *Escherichia coli.* Mol Microbiol. 2021.
811 doi:10.1111/mmi.14712

812 47. Mueller EA, Iken AG, Öztürk MA, Winkle M, Schmitz M, Vollmer W, et al. The active repertoire of *Escherichia*
813 *coli* peptidoglycan amidases varies with physiochemical environment. Mol Microbiol. 2021;116: 311–
814 328. doi:10.1111/mmi.14711

815 48. Aarsman MEG, Piette A, Fraipont C, Vinkenvleugel TMF, Nguyen-Distèche M, Blaauwen T den. Maturation of
816 the *Escherichia coli* divisome occurs in two steps. Mol. Microbiol. 2005;55: 1631–1645.
817 doi:10.1111/j.1365-2958.2005.04502.x

818 49. Perez AJ, Cesbron Y, Shaw SL, Villicana JB, Tsui H-CT, Boersma MJ, et al. Movement dynamics of divisome
819 proteins and PBP2x:FtsW in cells of *Streptococcus pneumoniae*. Proc. Natl Acad Sci. USA. 2019;116:
820 3211–3220. doi:10.1073/pnas.1816018116

821 50. Monteiro JM, Pereira AR, Reichmann NT, Saraiva BM, Fernandes PB, Veiga H, et al. Peptidoglycan synthesis
822 drives an FtsZ-treadmilling-independent step of cytokinesis. Nature. 2018;554: 528–532.
823 doi:10.1038/nature25506

824 51. Tsang M-J, Bernhardt TG. A role for the FtsQLB complex in cytokinetic ring activation revealed by an ftsL allele
825 that accelerates division. Mol. Microbiol. 2014. doi:10.1111/mmi.12905

826 52. Bernard CS, Sadasivam M, Shiomi D, Margolin W. An altered FtsA can compensate for the loss of essential cell
827 division protein FtsN in *Escherichia coli*. Mol. Microbiol. 2007;64: 1289–1305. doi:10.1111/j.1365-
828 2958.2007.05738.x

829 53. Boes A, Olatunji S, Breukink E, Terrak M. Regulation of the Peptidoglycan Polymerase Activity of PBP1b by
830 Antagonist Actions of the Core Divisome Proteins FtsBLQ and FtsN. Blaauwen T den, Salama NR, editors.
831 mBio. 2019;10: e01912-18. doi:10.1128/mbio.01912-18

832 54. Blaauwen T den, Luirink J. Checks and Balances in Bacterial Cell Division. Mbio. 2019;10.
833 doi:10.1128/mbio.00149-19

834 55. Korat B, Mottl H, Keck W. Penicillin-binding protein 4 of *Escherichia coli*: molecular cloning of the *dacB* gene,
835 controlled overexpression, and alterations in murein composition. Mol. Microbiol. 1991;5: 675–684.

836 56. Harris F, Brandenburg K, Seydel U. Investigations into the mechanisms used by the C-terminal anchors of
837 *Escherichia coli* penicillin-binding proteins 4, 5, 6 and 6b for membrane interaction. Eur.J. Biochem.
838 2002. doi:10.1046/j.1432-1033.2002.03295.x

839 57. Pedro MAD, Schwarz U. Heterogeneity of newly inserted and preexisting murein in the sacculus of *Escherichia*
840 *coli*. Proceedings of the Proc. Natl Acad Sci. USA. 1981;78: 5856–5860.

841 58. Iwaya M, Strominger JL. Simultaneous deletion of D-alanine carboxypeptidase IB-C and penicillin-binding
842 component IV in a mutant of E*scherichia coli* K12. Proc. Natl Acad Sci. USA. 1977;74: 2980–2984.
843 doi:10.1073/pnas.74.7.2980

844 59. Nelson DE, Young KD. Contributions of PBP 5 and DD-carboxypeptidase penicillin binding proteins to
845 maintenance of cell shape in *Escherichia coli.* J. Bacteriol. 2001;183: 3055–3064.
846 doi:10.1128/jb.183.10.3055-3064.2001

847 60. Kishida H, Unzai S, Roper DI, Lloyd A, Park S-Y, Tame JRH. Crystal Structure of Penicillin Binding Protein 4
848 (*dacB)* from *Escherichia coli*, both in the Native Form and Covalently Linked to Various Antibiotics.
849 Biochemistry. 2006;45: 783–792. doi:10.1021/bi051533t

850 61. Thunnissen MMGM, Fusetti F, Boer BD, Dijkstra BW. Purification, crystallisation and preliminary X-ray analysis
851 of penicillin binding protein 4 from *Escherichia coli,* a protein related to class a β-lactamases. J. Mol. Biol.
852 1995;247: 149–153. doi:10.1006/jmbi.1994.0128

853 62. Clarke TB, Kawai F, Park S-Y, Tame JRH, Dowson CG, Roper DI. Mutational analysis of the substrate specificity
854 of *Escherichia coli* penicillin binding protein 4. Biochemistry. 2009;48: 2675–2683.
855 doi:10.1021/bi801993x

856 63. Hocking J, Priyadarshini R, Takacs CN, Costa T, Dye NA, Shapiro L, et al. Osmolality-Dependent Relocation of
857 Penicillin-Binding Protein PBP2 to the Division Site in *Caulobacter crescentus*. J.Bacteriol. 2012;194:
858 3116–3127. doi:10.1128/jb.00260-12

859 64. Consoli E, Collet J-F, Blaauwen T den. The *Escherichia coli* Outer Membrane β-Barrel Assembly Machinery
860 (BAM) Anchors the Peptidoglycan Layer by Spanning It with All Subunits. Int. J. Mol. Sci. 2021;22: 1853.
861 doi:10.3390/ijms22041853

862 65. Liu X, Meiresonne NY, Bouhss A, Blaauwen T den. FtsW activity and lipid II synthesis are required for
863 recruitment of MurJ to midcell during cell division in *Escherichia coli.* Mol. Microbiol. 2018;109: 855–
864 884. doi:10.1111/mmi.14104

865 66. Alcorlo M, Dik DA, Benedetti SD, Mahasenan KV, Lee M, Domínguez-Gil T, et al. Structural basis of denuded
866 glycan recognition by SPOR domains in bacterial cell division. Nature Commun.. 2019;10: 5567–13.
867 doi:10.1038/s41467-019-13354-4

868 67. Sykes RB, Bonner DP, Bush K, Georgopapadakou NH. Azthreonam (SQ 26,776), a synthetic monobactam
869 specifically active against aerobic gram-negative bacteria. Antimicrob Agents Ch. 1982;21: 85–92.
870 doi:10.1128/aac.21.1.85

871 68. Nanninga N. Cell division and peptidoglycan assembly in *Eschenchia coli.* Mol. Microbiol. 1991;5: 791–795.
872 doi:10.1111/j.1365-2958.1991.tb00751.x

873 69. Pedro MAD, Quintela JC, Höltje JV, Schwarz H. Murein segregation in *Escherichia coli*. J. Bacteriol. 1997;179:
874 2823–2834.

875 70. Banzhaf M, Saparoea B van den B van, Terrak M, Fraipont C, Egan A, Philippe J, et al. Cooperativity of
876 peptidoglycan synthases active in bacterial cell elongation. Mol. Microbiol. 2012;85: 179–194.
877 doi:10.1111/j.1365-2958.2012.08103.x

878 71. Jean NL, Bougault CM, Lodge A, Derouaux A, Callens G, Egan AJF, et al. Elongated structure of the outer-
879 membrane activator of peptidoglycan synthesis LpoA: implications for PBP1A stimulation. Structure
880 (London, England : 1993). 2014;22: 1047–1054. doi:10.1016/j.str.2014.04.017

881 72. Jean NL, Bougault C, Derouaux A, Callens G, Vollmer W, Simorre J-P. Backbone and side-chain (1)H, (13)C, and
882 (15)N NMR assignments of the N-terminal domain of *Escherichia coli* LpoA. Biomolecular NMR
883 assignments. 2015;9: 65–69. doi:10.1007/s12104-014-9546-2

884 73. Typas A, Banzhaf M, Saparoea B van den B van, Verheul J, Biboy J, Nichols RJ, et al. Regulation of
885 peptidoglycan synthesis by outer-membrane proteins. Cell. 2010;143: 1097–1109.
886 doi:10.1016/j.cell.2010.11.038

887 74. Goehring NW, Beckwith J. Diverse paths to midcell: assembly of the bacterial cell division machinery. Current
888 Biology : CB. 2005;15: R514-26. doi:10.1016/j.cub.2005.06.038

889 75. Ting S-Y, Bosch DE, Mangiameli SM, Radey MC, Huang S, Park Y-J, et al. Bifunctional Immunity Proteins
890 Protect Bacteria against FtsZ-Targeting ADP-Ribosylating Toxins. Cell. 2018;175: 1380-1392.e14.
891 doi:10.1016/j.cell.2018.09.037

892 76. Koppelman C-M, Aarsman MEG, Postmus J, Pas E, Muijsers AO, Scheffers D-J, et al. R174 of *Escherichia coli*
893 FtsZ is involved in membrane interaction and protofilament bundling, and is essential for cell division.
894 Mol. Microbiol. 2004;51: 645–657.

895 77. Pichoff S, Du S, Lutkenhaus J. Disruption of divisome assembly rescued by FtsN-FtsA interaction in *Escherichia*
896 *coli*. Proc. Natl Acad Sci. USA. 2018;115: E6855–E6862. doi:10.1073/pnas.1806450115

897 78. Du S, Henke W, Pichoff S, Lutkenhaus J. How FtsEX localizes to the Z ring and interacts with FtsA to regulate
898 cell division. Mol. Microbiol. 2019. doi:10.1111/mmi.14324

899 79. Arends SJR, Kustusch RJ, Weiss DS. ATP-binding site lesions in FtsE impair cell division. J. Bacteriol. 2009;191:
900 3772–3784. doi:10.1128/jb.00179-09

901 80. Vischer NOE, Verheul J, Postma M, Saparoea B van den B van, Galli E, Natale P, et al. Cell age dependent
902 concentration of *Escherichia coli* divisome proteins analyzed with ImageJ and ObjectJ. Front. Microbiol.
903 2015;6: 586. doi:10.3389/fmicb.2015.00586

904 81. Jensen KF. The Escherichia coli K-12 “wild types” W3110 and MG1655 have an rph frameshift mutation that
905 leads to pyrimidine starvation due to low pyrE expression levels. J Bacteriol. 1993;175: 3401–3407.
906 doi:10.1128/jb.175.11.3401-3407.1993

907 82. Potluri L-P, Kannan S, Young KD. ZipA is required for FtsZ-dependent preseptal peptidoglycan synthesis prior
908 to invagination during cell division. J. Bacteriol. 2012;194: 5334–5342. doi:10.1128/jb.00859-12

909 83. Datsenko KA, Wanner BL. One-step inactivation of chromosomal genes in *Escherichia coli* K-12 using PCR
910 products. Proc. Natl Acad Sci. USA. 2000;97: 6640–6645. doi:10.1073/pnas.120163297

911 84. Chen JC, Weiss DS, Ghigo J-M, Beckwith J. Septal Localization of FtsQ, an Essential Cell Division Protein in
912 *Escherichia coli*. J Bacteriol. 1999;181: 521–530. doi:10.1128/jb.181.2.521-530.1999

913 85. Alexeeva S, Gadella TWJ, Verheul J, Verhoeven GS, Blaauwen T den. Direct interactions of early and late
914 assembling division proteins in *Escherichia coli* cells resolved by FRET. Mol. Microbiol. 2010;77: 384–398.
915 doi:10.1111/j.1365-2958.2010.07211.x

916 86. Taschner PE, Huls PG, Pas E, Woldringh CL. Division behavior and shape changes in isogenic *ftsZ, ftsQ, ftsA*,
917 *pbpB*, and *ftsE* cell division mutants of *Escherichia coli* during temperature shift experiments. J Bacteriol.
918 1988;170: 1533–1540. doi:10.1128/jb.170.4.1533-1540.1988

919 87. Gibson DG, Young L, Chuang R-Y, Venter JC, Hutchison CA, Smith HO. Enzymatic assembly of DNA molecules
920 up to several hundred kilobases. Nat. Chem.Biol. 2009;6: 343–345. doi:10.1038/nmeth.1318

921 88. Buddelmeijer N, Aarsman M, Blaauwen T den. Immunolabeling of proteins in situ in *Escherichia coli* K12
922 strains. Bio-protocol. 2013;3: 1–5.

923 89. Ludwig C. Diffusion between unequally heated regions of initially uniform solutions. Sitzungsber Akad Wiss
924 Wien Math-Naturwiss K1. 1856;20: 593.

925 90. Jerabek-Willemsen M, Wienken CJ, Braun D, Baaske P, Duhr S. Molecular interaction studies using microscale
926 thermophoresis. Assay and drug develop. technol. 2011;9: 342–353. doi:10.1089/adt.2011.0380

927 91. Müller P, Ewers C, Bertsche U, Anstett M, Kallis T, Breukink E, et al. The essential cell division protein FtsN
928 interacts with the murein (peptidoglycan) synthase PBP1B in *Escherichia coli.* J. Biol. Chem. 2007;282:
929 36394–36402. doi:10.1074/jbc.m706390200

930 92. Glauner B. Separation and quantification of muropeptides with high-performance liquid chromatography.
931 Anal. Biochem. 1988;172: 451–464. doi:10.1016/0003-2697(88)90468-x

932 93. laue T, Shah B, Ridgeway T, Pelletier S. Computer-aided interpretation of analytical sedimentation data for
933 proteins. Royal Soc. Chem. 1992;90: 125.

934 94. Schuck P. Size-distribution analysis of macromolecules by sedimentation velocity ultracentrifugation and
935 lamm equation modeling. Biophys. J. 2000;78: 1606–1619. doi:10.1016/s0006-3495(00)76713-0

936 95. Brookes E, Demeler B, Rosano C, Rocco M. The implementation of SOMO (SOlution MOdeller) in the
937 UltraScan analytical ultracentrifugation data analysis suite: enhanced capabilities allow the reliable
938 hydrodynamic modeling of virtually any kind of biomacromolecule. Eur. Biophys. J.: EBJ. 2010;39: 423–
939 435. doi:10.1007/s00249-009-0418-0

940 96. Ursinus A, Ent F van den, Brechtel S, Pedro M de, Höltje J-V, Löwe J, et al. Murein (peptidoglycan) binding
941 property of the essential cell division protein FtsN from *Escherichia coli.* J. Bacteriol. 2004;186: 6728–
942 6737. doi:10.1128/jb.186.20.6728-6737.2004

943 97. Bertsche U, Breukink E, Kast T, Vollmer W. In vitro murein peptidoglycan synthesis by dimers of the
944 bifunctional transglycosylase-transpeptidase PBP1B from *Escherichia coli*. J. Biol. Chem. 2005;280:
945 38096–38101. doi:10.1074/jbc.m508646200

946 98. Casadaban MJ, Cohen SN. Analysis of gene control signals by DNA fusion and cloning in *Escherichia coli*. J.
947 Mol. Biol. 1980;138: 179–207. doi:10.1016/0022-2836(80)90283-1

948 99. Ishino F, Jung HK, Ikeda M, Doi M, Wachi M, Matsuhashi M. New mutations fts-36, lts-33, and ftsW clustered
949 in the mra region of the *Escherichia coli* chromosome induce thermosensitive cell growth and division. J.
950 Bacteriol. 1989;171: 5523–5530.

951 100. Baba T, Ara T, Hasegawa M, Takai Y, Okumura Y, Baba M, et al. Construction of Escherichia coli K-12 in-
952 frame, single-gene knockout mutants: the Keio collection. Mol. Syst. Biol.. 2006;2: 2006.0008.
953 doi:10.1038/msb4100050

954

955

956

957

958

959

960

961

962 **TABLE 1 Strain and plasmids used in this study.**

Strain	Mutation	Genotype	Source
LMC500 (MC4100)	Wild-type	F^-, *araD139, Δ(argF-lac)U169, deoC1, flbB5301, lysA1, ptsF25, rbsR, relA1, rpsL150*	[86]
BL21(DE3)	Overexpression strain	F^- *ompT, dcm lon hsdS hsdSB(rB-mB-)* λ(DE3)	Novagen
BW25113	Keio background strain	*F^-, Δ(araD-araB)567, lacZ4787(del)::rrnB-3, LAM-, rph-1, Δ(rhaD-rhaB)568, hsdR514*	[83]
DH5α	Storage strain	F^- *endA1 glnV44 thi-1 recA1* φ80Δ*lacZ*ΔM15, $λ^-$	Invitrogen
MC1061	Laboratory strain	Δ(*araA-leu*)7697 Δ(*lac*)X74 *galK*16 *galE*15(GalS) $λ^-$e14- *mcrA*0 *relA1 rpsL*150(str^R) *spoT1 mcrB1 hsdR2*	[98]
LMC509	FtsZ (ts)	MC4100 *ftsZ*184	[86]
LMC511	FtsA (ts)	MC4100 *ftsA*10	[86]
LMC512	FtsA (ts)	MC4100 *ftsA*1882	[86]
LMC515	FtsE (ts)	MC4100 *ftsE*1181	[86]
LMC531	FtsQ (ts)	MC4100 *ftsQ*(ts)	[86]
LMC2487	FtsW (ts)	JLB17; F^- *thr, trp, his, thy, ara, lac, gal, xyl, mtl, rspL, tonA*, *ftsW* amino acid replacement G311D	[99]
LMC510	PBP3 (ts)	MC4100 *ftsI* 2158	[86]
BCB677	ΔPBP1A	BW25113Δ*mrcA*	[100]
BCB678	ΔPBP1B	BW25113Δ*mrcB*	[100]
BCB192	ΔLpoA	BW25113Δ*lpoA*	[100]
LMC2217	ΔLpoB	BW25113Δ*lpoA*	[100]
BCB655	ΔPBP4	BW25113Δ*dacB*	[100]
BCB1433	ΔPBP4	XWL010 MC4100Δ*dacB*	This work
BCB904	ΔNlpI	BW25113Δ*nlpI*	[100]
BCB1363	ΔPBP4ΔLpoA	BW25113Δ*dacB:kan*^{R}, Δ*lpoA*	This work
BCB744	ΔFtsE	BW25113Δ*ftsE* kan^R CAG60397	This work
BCB746	ΔFtsEX	BW25113Δ*ftsE*X cat^R CAG60399	This work
BCB1081	ΔFtsE 1-150	XL34 LMC500Δ*fts*E 1-150::*kan-fts*X	This work
BCB849	ΔFtsE 1-150	XL35 LMC500Δ*fts*E 1-150::*fts*X	This work
BCB1082	ΔFtsE	XL33 LMC500Δ*fts*E::-cam-p*Trc99A*down *fts*X	This work
BCB850	ΔFtsE	XL36 LMC500Δ*fts*E::p*Trc99A*down *fts*X	This work

Plasmid	Name	Characteristics	Source
pET21b	pET21b-PBP4(S62A)Δ1-60	Inactive PBP4 lacking residues 1-60, Amp^R	[3]

pET21b	pET21b-His-PBP4(S62A)Δ1-60	For purification of His-PBP4 (active site mutant), Amp^R	[3]
pET21b	pET21b-PBP4Δ1-60	Native PBP4 lacking residues 1-60, Amp^R	[3]
pET28a	pET28a-His-LpoA(sol)	Soluble LpoA (LpoAΔ1-27) construct, N-terminal His-tag, Kan^R	[71]
pET28a	pET28-His-$LpoA^N$	Purification of His-$LpoA^N$, Kan^R	[71]
pET28a	pET28-His-$LpoA^C$	Purification of His-$LpoA^C$, Kan^R	[71]
pTK1A-His	pTK1A-His	Full length His-PBP1A, Kan^R	[71]
pET28a-	pET28a-His-NlpI	Soluble NlpI construct, N-terminal His-tag, KanR	[6]
pBAD18	pBAD18-His-PBP4ΔD3	for purification of His- PBP4 lacking domain 3, Amp^R	This work
pBAD18	Tre1	Arabinose inducible Tre1, Amp^R	[75]
pBad18	Tre1 E415Q	TreE415Q inactive Tre1 variant, Amp^R	[75]
pXL86	pTHV mCh-FtsE wt	p*Trc* 99A down expressing mCh-FtsE(wt) colE1 ori, Amp^R	This work
pXL89	pTHV mCh-FtsE ts	p*Trc* 99A down expressing mCh-FtsE(ts) (P135S) colE1 ori, Amp^R	This work
pXL110	pSAV mNG-NNN-FtsE	p*Trc* 99A down expressing mNG-FtsE, p15A origin, Cam^R	This work
pXL133	pSAV-PBP4	p*Trc* 99A down expressing PBP4, p15A origin, Cam^R	This work
pXL134	pSAV-PBP4 S62G	p*Trc* 99A down expressing PBP4 S62G, p15A origin, Cam^R	This work
pXL135	pSAV-FtsE	p*Trc* 99A down expressing FtsE, p15A origin, Cam^R	This work
pXL137	pSAV-FtsE K41Q	p*Trc* 99A down expressing FtsE K41Q, p15A origin, Cam^R	This work
pXL138	pSAV-FtsE D162A	p*Trc* 99A down expressing FtsE D162A, p15A origin, Cam^R	This work
pXL139	pSAV-FtsE E163A	p*Trc* 99A down expressing FtsE E163A, p15A origin, Cam^R	This work
pXL140	pSAV-PBP4-ΔD3	p*Trc* 99A down expressing PBP4Δ173-247 (domain 3), p15A origin, Cam^R	This work
pXL150	pSAV-PBP4-D155A	p*Trc* 99A down expressing PBP4 D155A, p15A origin, Cam^R	This work
pXL151	pSAV-PBP4-R361A	p*Trc* 99A down expressing PBP4 R361A, p15A origin, Cam^R	This work

963 Amp^R, Kan^R and Cam^R are ampicillin, kananamycin and chloramphenicol resistance,

964 respectively

965

966

967 **TABLE 2 Primers used in this study.**

Primer	Sequence 5'-3'	Purpose
priXL51	ACCATGGCTAATTCCCATGTCAG	GA_pkd3_F
priXL54	GTGTAGGCTGGAGCTGCTTC	PCR_pkd3_R
priXL187	CCGGCCGAATTCAACAACAACTCGATGATTCGCTTTGAACATGTCAGC	FtsE-EcoRI fw
priXL188	GGCCAAGCTTTTATTCATGGCCCACGCCTCC	FtsE-EcoRI rv
priXL221	CATGAAGCCGTTGGCTTAACC	ΔFtsE-FA-F
priXL222	TAGGAACTTCGAAGCAGCTCCAGCCTACACTGTTAATCCTCTCGGGCAAAAAG	ΔFtsE -FA-R
priXL223	GGATATTCATATGGACCATGGCTAATTCCCATGTCAGGCGGTGGTGAACAAGCCCGC	ΔFtsE- 1-150
priXL224	GGTGAGCATGCGATAGGAACG	ΔFtsE-1:150
priXL225	TGAGCGGATAACAATTTCACACAGGAAACAGACCATGAATAAGCGCGATGCAATC	ΔFtsE-clean
priXL226	CTTTTCAGATCCTGCAATGCG	ΔFtsE-clean
priXL230	ATTCCGGCGCAGGGCAAAGTACTCTCCTGAAGCTG	FtsE-K41Q-F
priXL231	GATCAGCTTCAGGAGAGTACTTTGCCCTGCGCCGGA	FtsE-K41Q-R
priXL232	CGGTACTGCTAGCGGCTGAACCGACTGGTAACCTG	FtsE-D162A-F
priXL233	AGGTTACCAGTCGGTTCAGCCGCTAGCAGTACCGC	FtsE-D162A-R
priXL234	GTACTGCTAGCGGACGCTCCGACTGGTAACCT	FtsE-E163A-F
priXL235	AGGTTACCAGTCGGAGCGTCCGCTAGCAGTACCGC	FtsE-E163A-R
priXL236	AGATGGCGCTGCCTGCCGGCACCCAGAAAG	PBP4-S62G-F
priXL244	GCGCGAATTCatgCGATTTTCCAGATTTATCA	EcoRI-PBP4-F
priXL245	GCGCAAGCTTctaATTGTTCTGATAAATATC	HindIII-PBP4-R
priXL250	GTTGACCGCAACGGTGGCGGAAGCGGGTCTGTGCAGGATGGAGCCAGCTATG	PBP4ΔD3-F
priXL251	TCCATCCTGCACAGACCCGCTTCCGCCACCGTTGCGGTCAACTATGGCGGC	PBPΔD3-R
priXL266	CCGGCTGGCCATGGAATGCCATGACACAATGCTTTAGCGCTC	PBP4-D155A-F
priXL267	GGAGCGCTAAAGCATTGTGTCATGGCATTCCATGGCCAGCCGG	PBP4-D155A-R
priXL268	GCCGATGGTTCAGGGCTTTCGGCGCATAACCTGATTGCCCCCGCC	PBP4-R361A-F
priXL269	GGCGGGGGCAATCAGGTTATGCGCCGAAAGCCCTGAACCATCGGC	PBP4-R361A-R
prXW5-F	TAGTATGACGGCTCGATTCCAGGTTGTTAGCGCGAGATTgtgtaggctggagctgcttc	LMC500Δ*dacB*
priXW6-R	AATCTGAAGCCCCGGCCATGTGCCGGGGTTTCTTTTTGAatgggaattagccatggtcc	LMC500Δ*dacB*

968
969

Midcell localization of PBP4 of *Escherichia coli* modulates the timing divisome assembly

Jolanda Verheul[1#], Adam Lodge[2,7#], Hamish C.L. Yau[2,8#], Xiaolong Liu[1,9#], Xinwei Liu[1], Alexandra S. Solovyova[3], Athanasios Typas[4,5] Manuel Banzhaf[6*], Waldemar Vollmer[2**], and Tanneke den Blaauwen[1***]

[1]Bacterial Cell Biology, Swammerdam Institute for Life Sciences, Faculty of Science, University of Amsterdam; Science Park 904, 1098 XH Amsterdam, The Netherlands.
[2]Centre for Bacterial Cell Biology, Biosciences Institute, Newcastle University, Newcastle upon Tyne, NE2 4AX, United Kingdom.
[3]NUPPA, Leech Building, Framlington Place, Newcastle upon Tyne NE2 4HH, UK
[4]European Molecular Biology Laboratory, Genome Biology Unit, Heidelberg, Germany
[5]European Molecular Biology Laboratory, Structural & Computational Unit, Heidelberg, Germany
[6]Institute of Microbiology & Infection and School of Biosciences, University of Birmingham, Edgbaston, Birmingham, UK. B15 2TT
[7]Present address: Iksuda Therapeutics, The Biosphere, Draymans Way, Newcastle Helix, Newcastle upon Tyne, NE4 5BX, UK
[8]Pressent address: Procter & Gamble, Newcastle Innovation Centre, Whitley Road, Newcastle-Upon Tyne, NE12 9TS, UK.
[9]Department of Biochemistry, University of Oxford, OX1 3QU, Oxford, United Kingdom.

[#]contributed equally.
*Corresponding author. Tel: +44 121 4145586; Email: m.banzhaf@bham.ac.uk
**Corresponding author. Tel: +44 191 208 3216; Email: w.vollmer@ncl.ac.uk
***Corresponding author. Tel: +31 20 525 3852; Email: t.denblaauwen@uva.nl

FIGURES AND LEGENDS

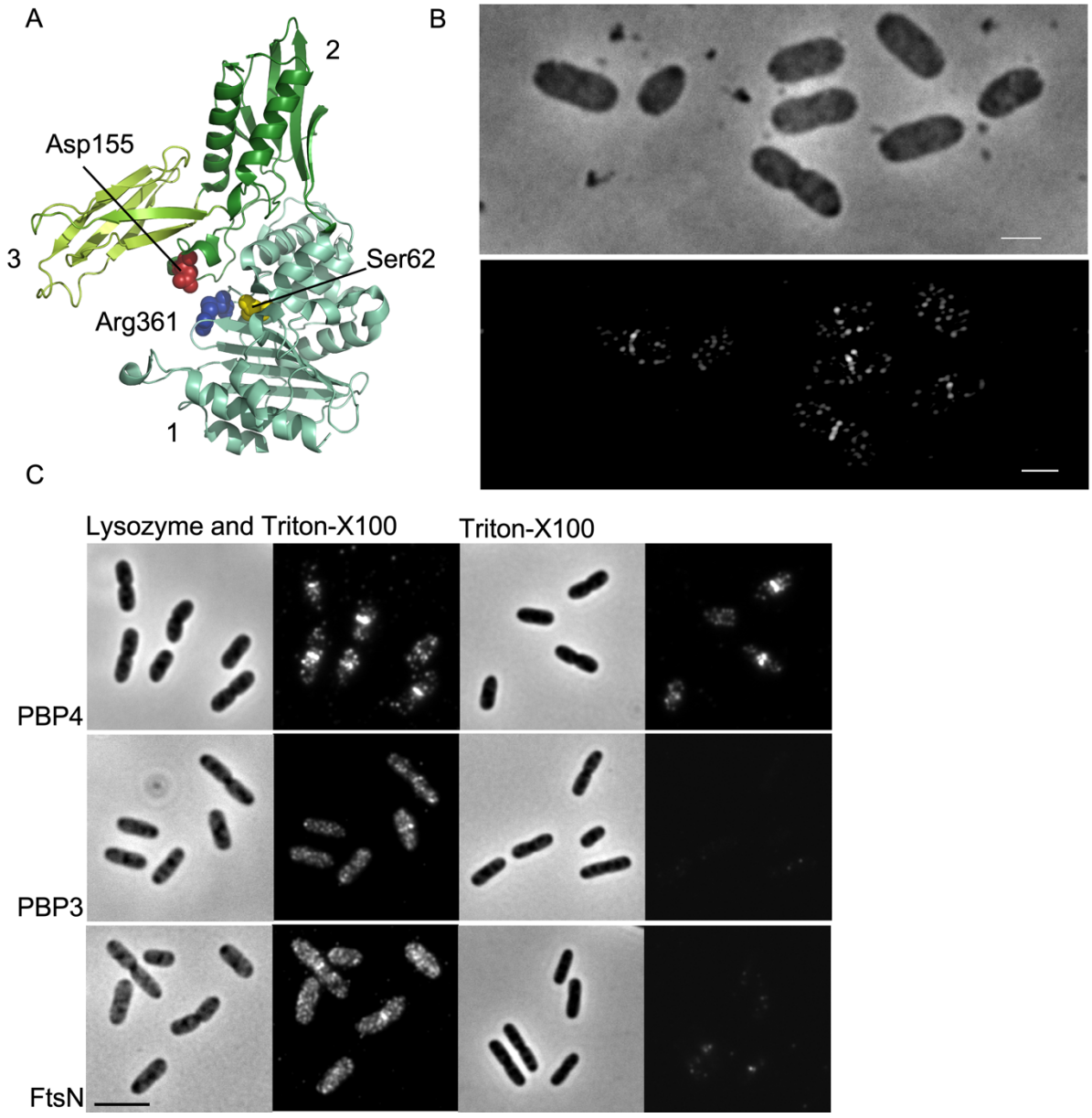

Fig 1. Structure of PBP4 and its localization at midcell and in the lateral wall during fast growth. A. Crystal structure of PBP4 in which the three domains (numbers 1-3) and some of the residues that are essential for its endopeptidase activity are indicated. B. MC4100 cells were grown exponentially in TY medium at 37°C to an OD600 of 0.3 and fixed and immunolabeled with BW25113Δ*dacB* pre-adsorpted anti-PBP4. Upper panel phase contrast image corresponding to the SIM fluorescence image in the lower panel. Scale bar equals 2 µm C. BW25113 wild-type cells were grown in TY at 37°C and harvested in the exponential phase

42 at an OD600 of 0.3 and fixed. Samples were divided into three aliquots and cells were
43 immunolabeled with antibodies against PBP3, FtsN and PBP4. The first aliquot was
44 immunolabeled without any treatment, the second after permeabilizing the cells with
45 TritonX-100 (right: phase contrast and fluorescence images) and the third after
46 permeabilizing cells with Triton-X100 and lysozyme (left: phase contrast and fluorescence
47 images). The scale bar equals 5 µm. PBP4, but not PBP3 or FtsN, is accessible without
48 degrading the peptidoglycan layer.

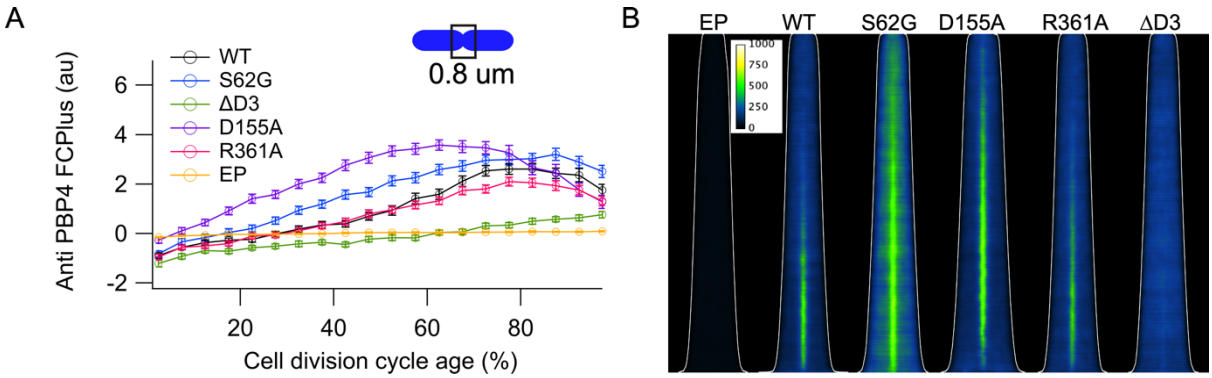

49

50 **Fig 2. Activity of PBP4 is not required for localization.** Cells were grown in minimal glucose
51 medium to steady state at 28°C, fixed and immunolabeled with antibodies against PBP4. (A)
52 The extra fluorescence at midcell (FCPlus) in the Δ*dacB* strain transformed with the empty
53 plasmid (EP, yellow), or plasmids expressing wild-type PBP4 (black), PBP4S63G (blue),
54 PBP4D155A, (purple) PBP4R361A (red), PBP4ΔD3 (green) was determined and plotted as
55 function of the cell division cycle age as in bins of 5% age classes with the error bar indicating
56 the 95% confidence interval. (B) Demographs of the localization fluorescence pattern of the
57 PBP4 variants shown in (A) with the cells sorted according to their cell length. The white line
58 indicates the length of the cells. Intensity scaling is identical for all maps. Number of cells
59 analyzed for each immunolabeling was at least 2000 cells.

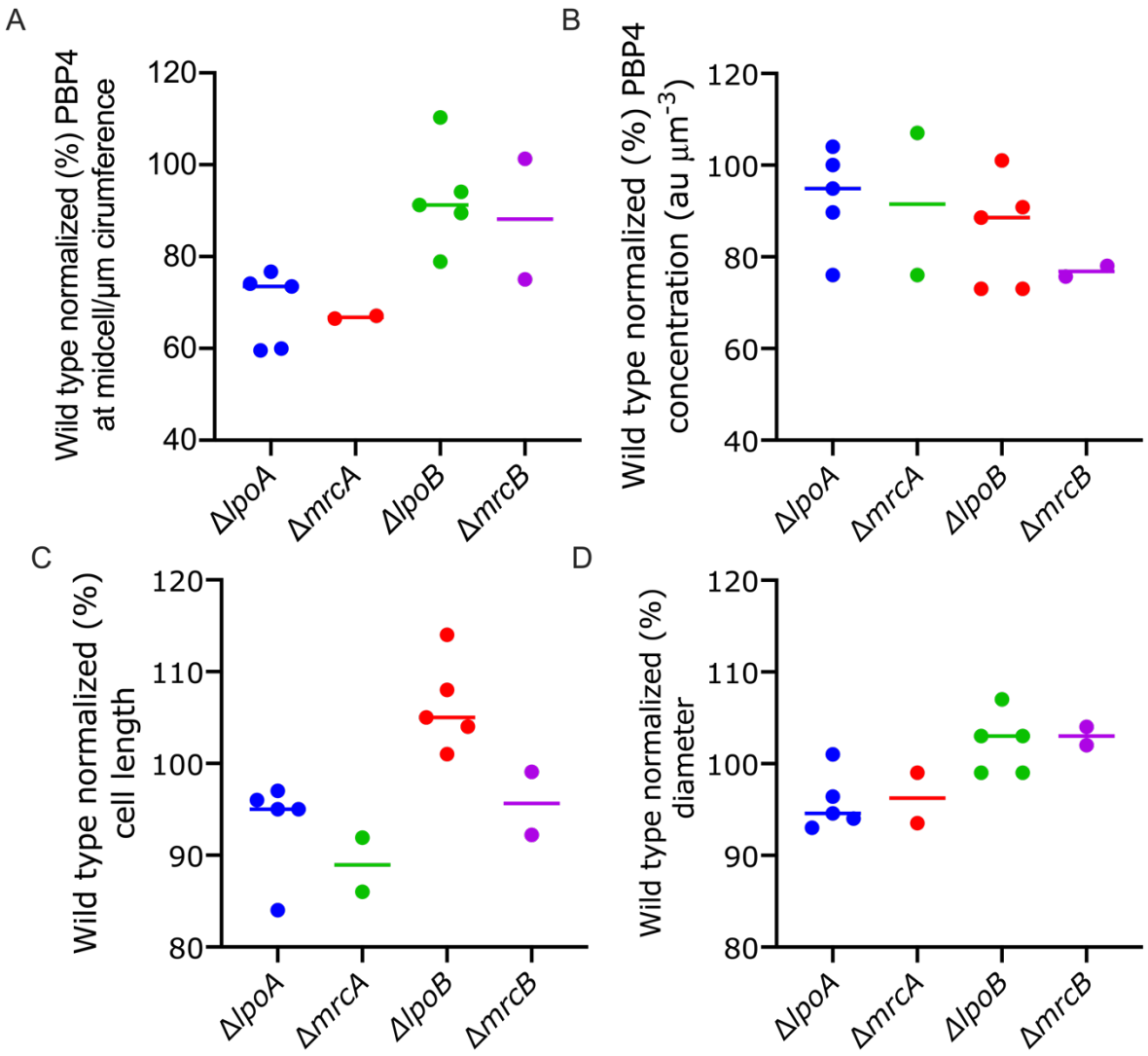

Fig 3. PBP1A and LpoA contribute to PBP4 midcell localization. Cells were grown exponentially to an OD of 0.3 in TY at 37°C, then fixed and immunolabeled with antibodies against PBP4. Because fluorescence imaging by microscopes is usually not directly comparable between different experiments, all results in each experiment were normalized to the parental strain BW25113. (A) PBP4 fluorescence at midcell per µm circumference of the cell. (B) Concentration of PBP4 in the cells. (C) length of the cells. (D) Diameter of the cells. Δ*lpoA* (n=5), Δ*lpoB* (n=5), Δ*mrcA* (PBP1A, n=2), Δ*mrcB* (PBP1B, n=2). Each point is the average of 1000-2000 cells. Based on the one-way Anova the difference in midcell localization is

69 significant (P=0.009) while the difference in concentration of PBP4 is not significant

70 (P=0.0484).

71

72 A

73

	K_D of interactions (nM)	
Ligand	PBP4	PBP4ΔD3
LpoA	315 ± 38	153 ± 31
$LpoA^C$	226 ± 15	315 ± 21
$LpoA^N$	954 ± 52	17 ± 4
NlpI	177 ± 49	n.d.[1]
PBP1A	67 ± 9	240 ± 50

[1] no interaction detected.

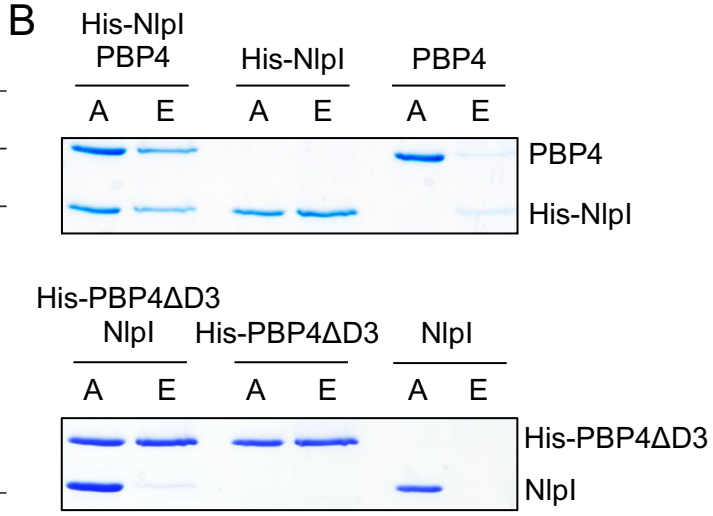

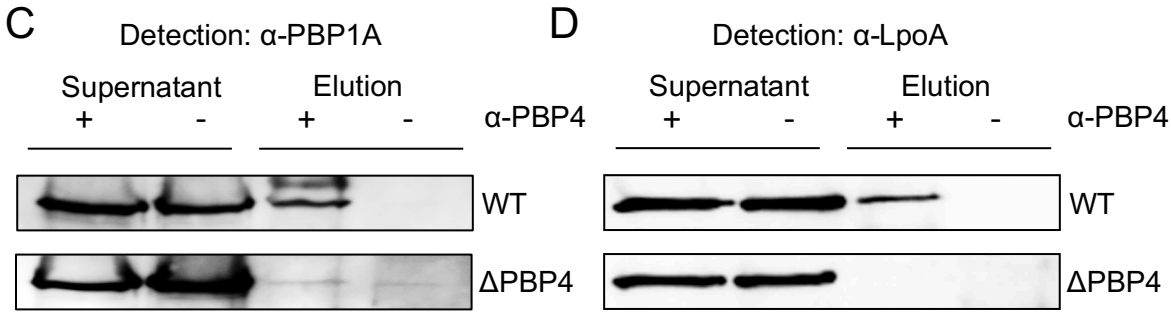

84 **Fig 4. PBP4 interacts with PBP1A, LpoA and NlpI.** (A) Summary of apparent K_D values of the

85 interactions of PBP4 or a version lacking domain 3 (PBP4ΔD3) with LpoA, the C-terminal

86 domain of LpoA ($LpoA^C$), the N-terminal domain of LpoA ($LpoA^N$), NlpI and PBP1A determined

87 by microscale thermophoresis (MST). Corresponding binding curves are shown in Suppl.

88 Figure S7. (B) Pulldown experiment showing that domain 3 of PBP4 is required for interaction

89 with NlpI. Oligo-histidine tagged NlpI (His-NlpI) pulled down PBP4 to Ni-NTA beads. His-tagged

90 PBP3ΔD3 did not pull down untagged NlpI. A, applied sample; E, eluted sample. (C) *In vivo*

91 cross-linking/co-immunoprecipitation showing interaction between PBP1A and PBP4.

92 Growing cells of BW25113 (wt) or BW25113Δ*dacB* (ΔPBP4) were chemically cross-linked with

93 DTSSP and cell extract was immunoprecipitated with purified anti-PBP4 antibody. Control
94 samples did not receive anti-PBP4 antibody. The cross-linker was cleaved by reducing agent
95 and proteins were separated by SDS-PAGE and transferred to a membrane, followed by
96 detection of PBP1A with specific antibodies. PBP1A was detected in the elution of the sample
97 from wild-type and not from ΔPBP4. (D) *In vivo* cross-linking/co-immunoprecipitation (as in
98 panel C) showing that PBP4 and be cross-linked with LpoA in cells.
99

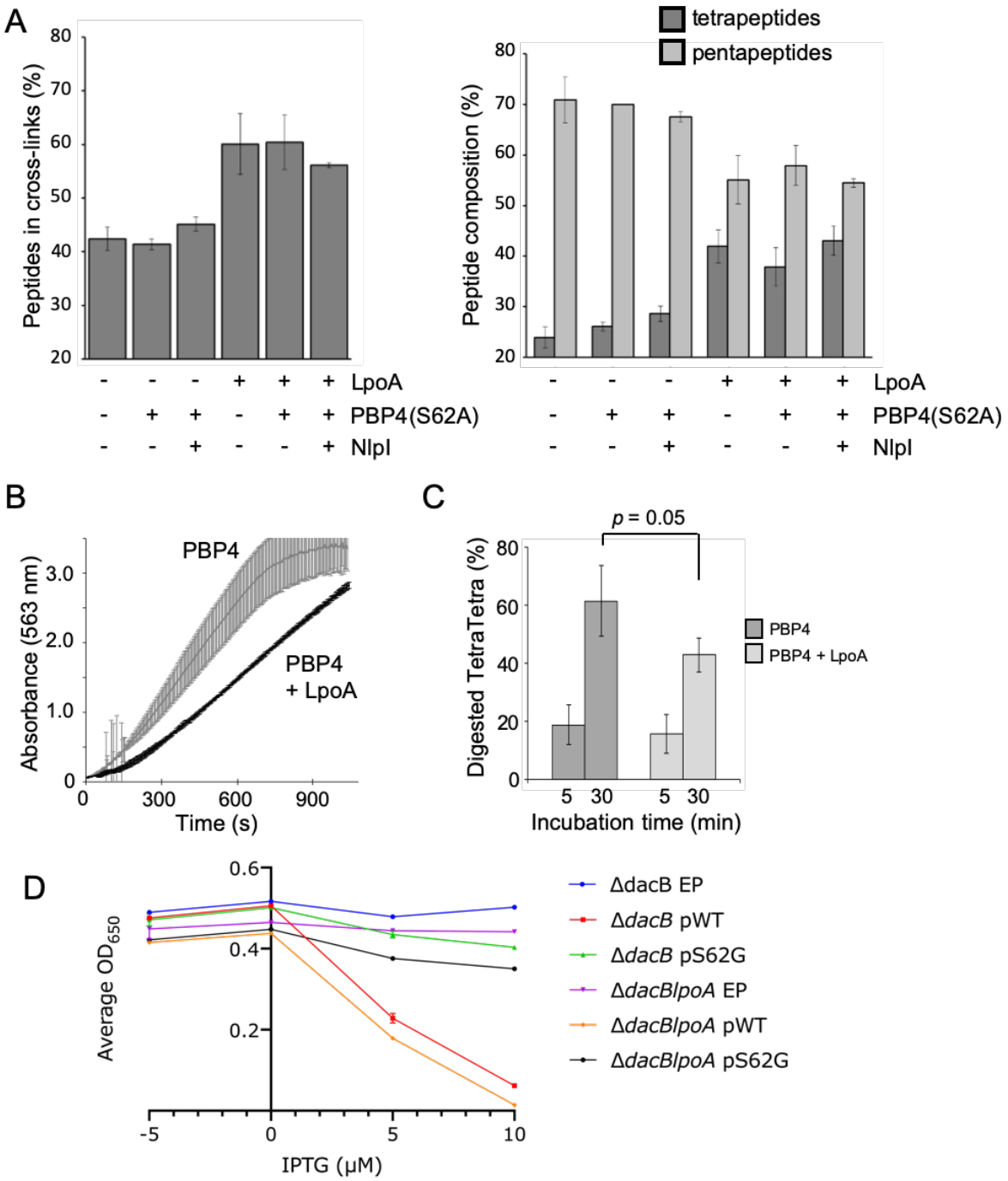

Fig 5 PBP4 or NlpI do not affect the activity of PBP1A whereas LpoA reduces the activity of PBP4. (A) Summary of the results from an *in vitro* PG synthesis assay with PBP1A (in the presence or absence of LpoA) and radio-labelled lipid II substrate. The presence of NlpI, catalytically inactive PBP4(S62A) or both together, does not affect the cross-linkage of the PG product of a PBP1A or PBP1A/LpoA reaction (left side), and NlpI, PBP4(S62A) or both together,

106 don't induce enhanced carboxypeptidase activity of PBP1A, which would be seen as a higher
107 content of tetrapeptides (right side). Values are mean ± variation of two independent repeats.
108 Example chromatograms are shown in Figure S8. (B) The presence of LpoA modestly reduces
109 the activity of PBP4 in a DD-carboxypeptidase assay using the substrate *N*-acetyl-L-Lys-D-Ala-
110 D-Ala. (C) LpoA also reduces slightly the activity of PBP4 against PG sacculi from BW25113, as
111 seen by the reduced digestion of TetraTetra upon a 30 min incubation period.
112 (D The Δ*dacB* and Δ*dacB*Δ*lpoA* mutant strains are equally sensitive to overexpression of PBP4.
113 The average growth over time as measured by OD650 nm is plotted against the added IPTG
114 concentration. The culture grown in TY with glucose to suppress the expression is represented
115 by -5 on the X-axe. All other data points are from cell grown in TY without glucose (n=4).
116

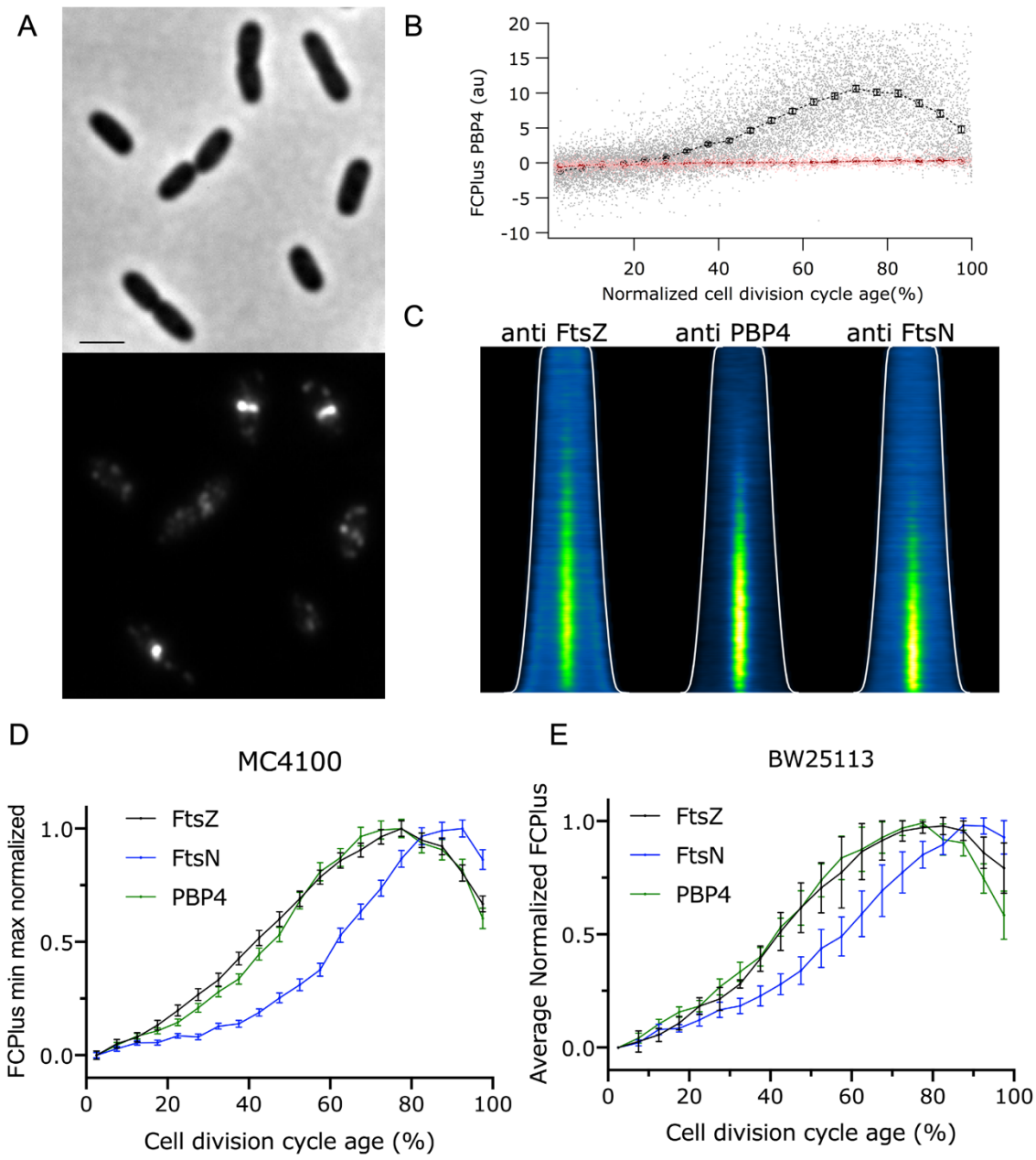

Fig 6 Cell division cycle timing of the localization of PBP4. (A) MC4100 cells were grown to steady state in minimal glucose medium at 28°C and immunolabeled with antibodies specific for PBP4. Phase contrast (top) and fluorescence is shown (bottom). Scale bar equals 2 µm. (B) The extra fluorescence at midcell compared to the rest of the cell (FCPlus) is plotted as function of the normalized cell division cycle age. The dots (grey for MC4100 and light pink for the BW25113 Δ*dacB strain*) are the values measured for the individual cells and the markers with bars (black for the wild-type MC4100, red for the BW25113 Δ*dacB*) are 5% age

125 bins with 95% confidence. (C) Demographs of the localization of FtsZ, PBP4 and FtsN in the
126 cells sorted according to cell length. The white line indicates the length of the cells. (D)
127 Comparison of the timing of the localization at midcell of FtsZ (black), PBP4 (green) and FtsN
128 (blue) during the cell division cycle age. The FCPlus values are min-max normalized to enable
129 timescale comparison, despite differences in molecule number and antibody affinities. (E)
130 BW25113 wild type cells were grown to steady state in minimal glucose medium at 28°C and
131 immunolabeled with antibodies specific for FtsZ, PBP4 and FtsN. The FCPlus of three
132 independent biological experiments in 5% age bins was determined. The binned FCPlus values
133 were min-max normalized. The average min-max normalized FCPlus values of the three
134 experiments were subsequently plotted as function of the cell division cycle.

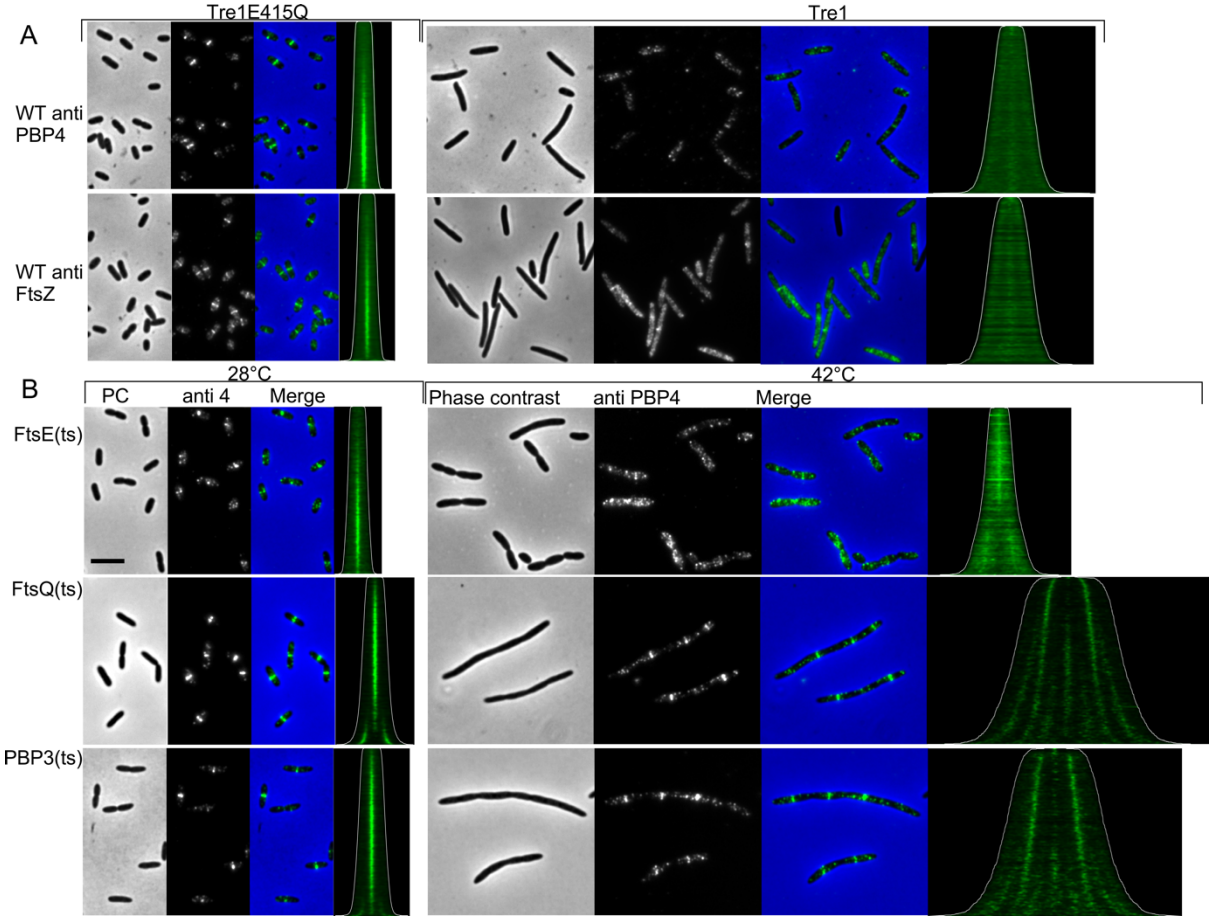

135

136 **Fig 7 PBP4 localization is dependent on the presence of the proto-ring. A.** MC4100 was
137 transform with a plasmid that expressed either Tre1 that abolished the ability of FtsZ to

138 polymerize by ADP-ribosylation of residue R174 or with the inactive variant Tre1(E415Q). Cells
139 were grown in Gb1 medium at 28°C and expression of the inhibitor was induced for 2 mass
140 doublings (MD) with 0.15% arabinose. Subsequently, the cells were fixed and immunolabeled
141 with antibodies against FtsZ or PBP4. From left to right: the phase contrast (PC),
142 corresponding fluorescence image of the PBP4 labeling and the merged images ate shown. In
143 the demographs the cells are sorted according to cell length (contours in white). The number
144 of cells analyzed were 3694 and 3756 for Tre1E415Q and 1275 and1621 for Tre1 for anti FtsZ
145 and anti PBP4, respectively. **B.** Isogenic strains of MC4100 producing different temperature
146 sensitive (ts) versions of cell division proteins were grown to steady state in Gb1 medium at
147 28°C and split in two parts. These were 1:4 diluted in prewarned medium and grown for two
148 MD at either 28°C or 42°C. The cells were fixed, labeled with antibodies specific for PBP4 (a4).
149 From left to right: the phase contrast (PC), corresponding fluorescence image of the PBP4
150 labeling and the merged images at the permissive temperature, demograph of PBP4
151 fluorescence localization where cells are sorted according to their cell length (contours in
152 white). This is followed by the same series from the non-permissive temperature samples.
153 The number of cells analyzed were 2809 and 1576 for LMC515 FtsE(ts), 3833 and 1203 for
154 LMC531 FtsQ (ts) and 3876 and 926 for LMC510 PBP3(ts), for the cells grown at 28°C and 42°C,
155 respectively. The scale bar equals 5 µm. Within one antibody staining the brightness and
156 contrast of the samples is identical and therefore directly comparable.

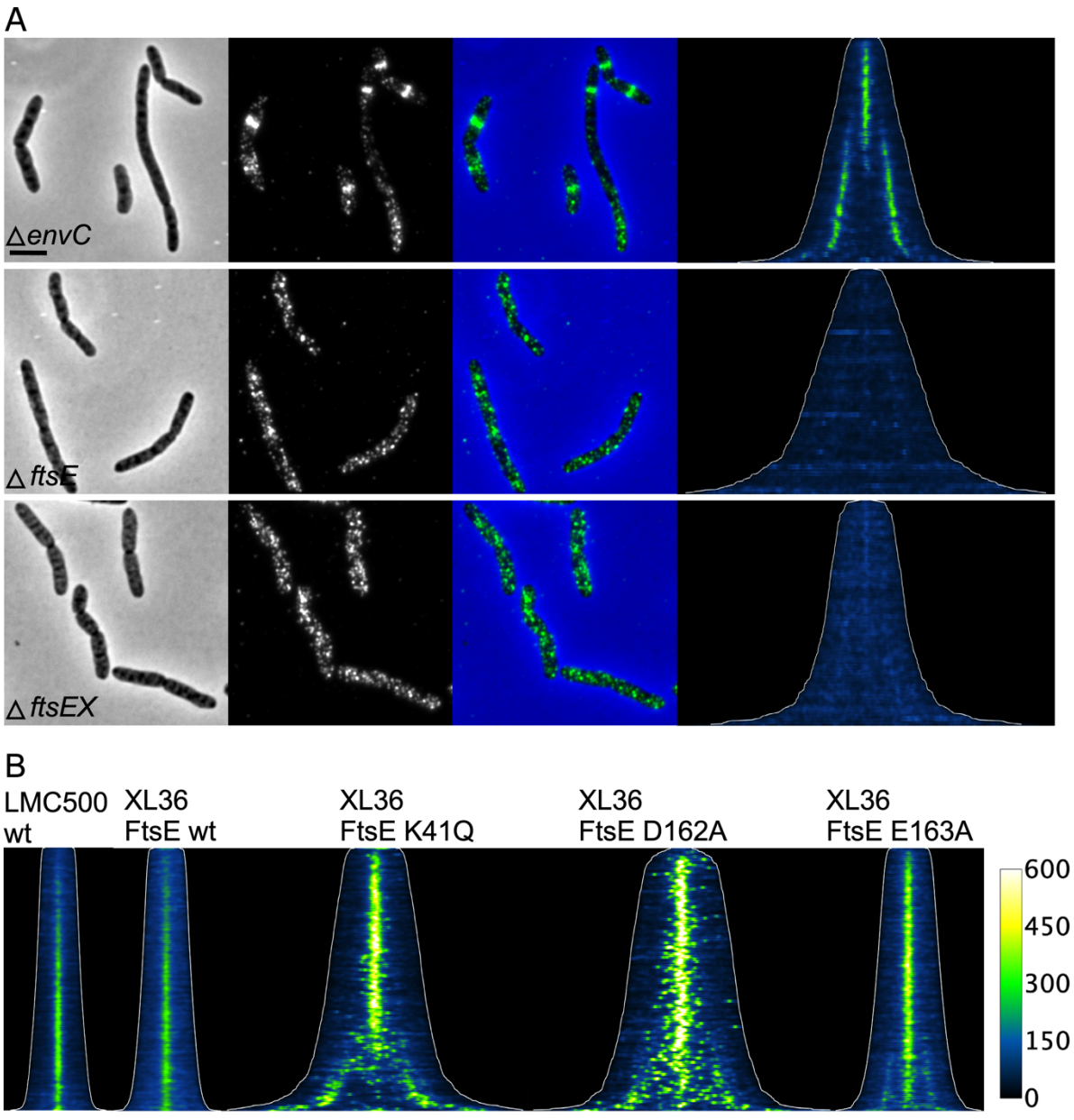

157

158 **Fig 8 PBP4 is recruited by the septal cleavage complex FtsEX.** (A) Cells of BW25113 expressing

159 the proteins indicated were grown in LB at 37°C to OD_{600} = 0.3, fixed and labeled with specific

160 antibodies against PBP4. From left to right, the phase contrast, corresponding fluorescence

161 image of the PBP4 labeling, and the merged former two images, map of fluorescence with the

162 cell lengths outlined (with the same contrast and brightness for all maps) of PBP4 localization

163 where cells are sorted according to their cell length are shown. The number of cells analyzed

164 were 687 for Δ*envC*, 434 for Δ*ftsE*, and 346 for Δ*ftsEX*. The scale bar equals 5 μm. (B) Cells of

165 LMC500 or XL36 (LMC500Δ*ftsE*::p*Trc99A*down *fts*X) expressing wild-type or active site

166 versions of FtsE were immunolabeled with anti-PBP4 antibodies. Cells were grown in TY at
167 30°C and FtsE expression from plasmid was induced for 2 mass doubling with 30 µM IPTG,
168 and cell were fixed and harvested at an OD_{600} of 0.3. The maps of PBP4 fluorescence with the
169 cell lengths outlined is shown for the indicated strains. Number of cells analyzed: LMC500
170 (2462), (wt) (2588), K41Q (728), D162A (554), and E163E (1052).
171

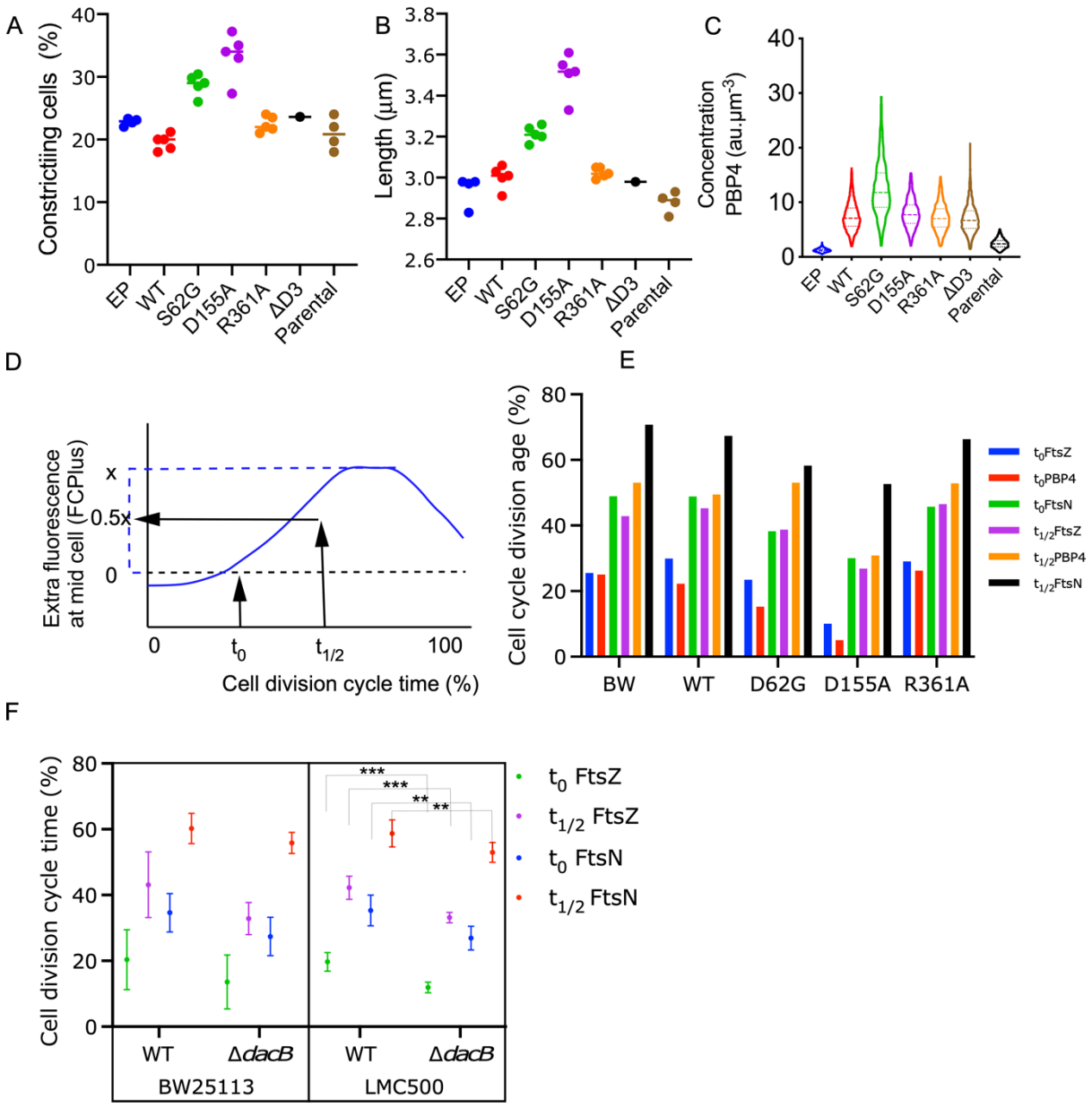

172

173 **Fig 9 Localization of PBP4 depends on the presence of domain 3 but not on activity.** Cells
174 were grown in minimal glucose medium to steady state at 28°C, fixed and immunolabeled
175 with the indicated antibodies. (A and B) Graphs with the percentage of constricting cells and
176 the average cell length in μm for the various mutants expressed from plasmid in the Δ*dacB*
177 strain and also of the parental strain BW24113 (n = 4). (C) The concentration of PBP4 in
178 fluorescent units per μm^3 in these cells for a representative experiment (out of the four
179 repeats).
180 (D) Graphical illustration of the meaning of t_0 and $t_{1/2}$. (E) Cell division cycle age timing of FtsZ,
181 PBP4, and FtsN for the parental strain BW25113, the Δ*dacB* strain carrying plasmids for the
182 expression of PBP4WT, PBP4S63G, PBP4D155A, or PBP4R361A. Plasmids were not induced.
183 (F). Cell division cycle age timing of FtsZ and FtsN for the Δ*dacB* strain and its parental
184 BW25113 (left) and the Δ*dacB* strain and its parental LMC500. P 0.0001 = ***, P 0.001 = **.
185 Number of points correspond to the number of independent biological replicates.
186

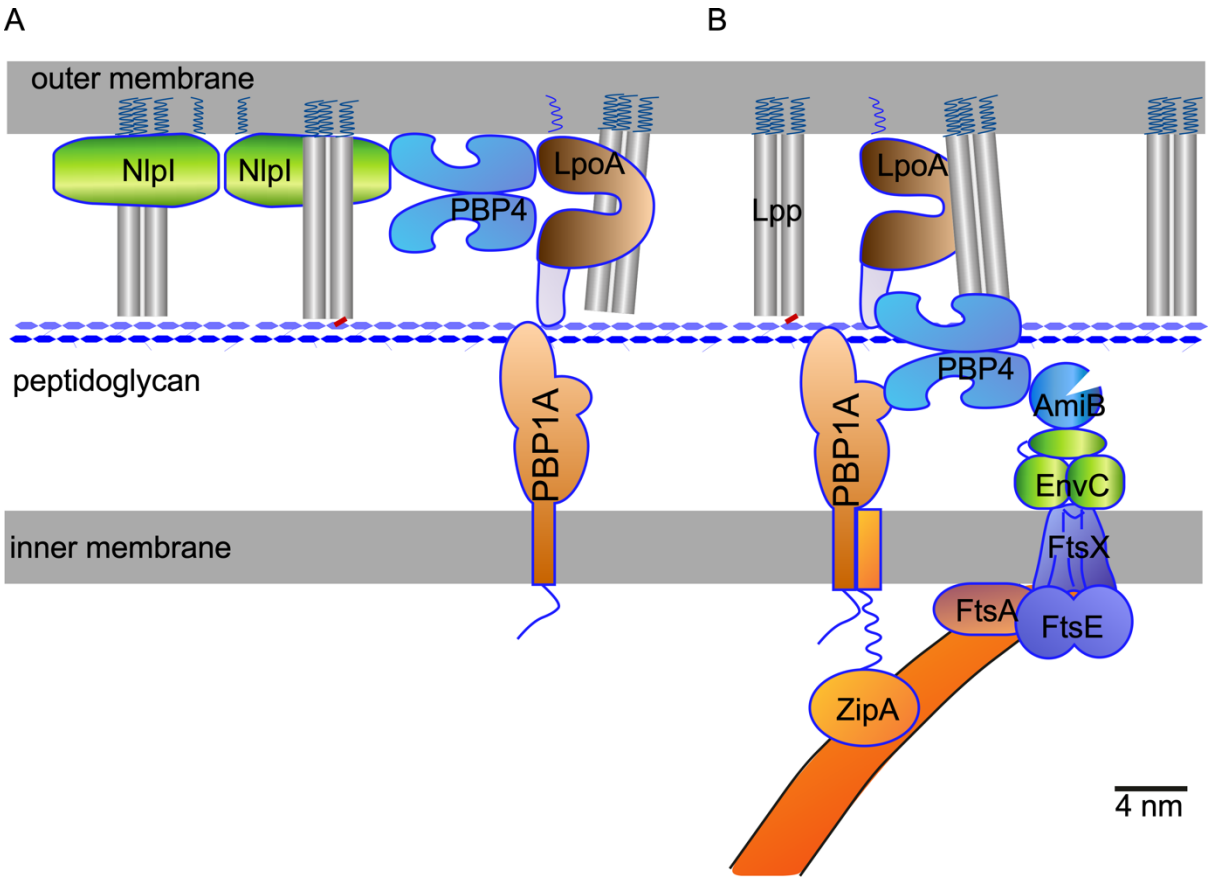

187

188

189 **Fig 10 Model of the organization of PBP4 in the periplasm of *E. coli*.** In a minimal medium

190 grown cell of average size of 3 by 0.86 µm 230000 Lpp trimeric proteins are present of which

191 1/3 is bound to PG. (A) During elongation PBP4 (or a fraction of the PBP4 molecules) is kept

192 away from its substrate through its interaction with NlpI and possibly LpoA. (B) PBP1A and

193 LpoA associate with ZipA and the Z-ring to assist in preseptal PG synthesis. Because of their

194 presence, the absence of NlpI and the newly synthesized PG, PBP4 is attracted by PBP1A and

195 LpoA. More PBP4 is accumulating at midcell and becoming clearly visible by immunolabeling

196 upon maturation of the divisome and synthesis of septal PG. All proteins apart from the FtsZ

197 polymer have been drawn according to their crystal structure shape and hydrated crystal

198 structure sizes (scale bar equals 4 nm). The membranes are assumed to be 2 nm and the

199 distance between the outer and the inner membrane 21 nm.

Midcell localization of PBP4 of *Escherichia coli* modulates the timing of divisome assembly

Jolanda Verheul[1#], Adam Lodge[2,7#], Hamish C.L. Yau[2,8#], Xiaolong Liu[1,9#], Xinwei Liu[1], Alexandra S. Solovyova[3], Athanasios Typas[4,5] Manuel Banzhaf[6*], Waldemar Vollmer[2**], and Tanneke den Blaauwen[1***]

[1]Bacterial Cell Biology, Swammerdam Institute for Life Sciences, Faculty of Science, University of Amsterdam; Science Park 904, 1098 XH Amsterdam, The Netherlands.
[2]Centre for Bacterial Cell Biology, Biosciences Institute, Newcastle University, Newcastle upon Tyne, NE2 4AX, United Kingdom.
[3]NUPPA, Leech Building, Framlington Place, Newcastle upon Tyne NE2 4HH, UK
[4]European Molecular Biology Laboratory, Genome Biology Unit, Heidelberg, Germany
[5]European Molecular Biology Laboratory, Structural & Computational Unit, Heidelberg, Germany
[6]Institute of Microbiology & Infection and School of Biosciences, University of Birmingham, Edgbaston, Birmingham, UK. B15 2TT
[7]Present address: Iksuda Therapeutics, The Biosphere, Draymans Way, Newcastle Helix, Newcastle upon Tyne, NE4 5BX, UK
[8]Pressent address: Procter & Gamble, Newcastle Innovation Centre, Whitley Road, Newcastle-Upon Tyne, NE12 9TS, UK.
[9]Department of Biochemistry, University of Oxford, OX1 3QU, Oxford, United Kingdom.

[#]contributed equally.
*Corresponding author. Tel: +44 121 4145586; Email: m.banzhaf@bham.ac.uk
**Corresponding author. Tel: +44 191 208 3216; Email: w.vollmer@ncl.ac.uk
***Corresponding author. Tel: +31 20 525 3852; Email: t.denblaauwen@uva.nl

Supplementary figures:

Figure S1. Preabsorption of antibodies against Δ*dacB* BW25113 strain results in PBP4 specific antibodies.
Figure S2. All PBP4 mutants are equally well expressed and only S62G is not able to bind Bocillin-FL.
Figure S3. PBP4ΔD3 binds beta-lactam but is inactive against PG substrates.
Figure S4. The absence of domain 3 does not affect the dimerization, secondary structure or PG binding of PBP4.
Figure S5. PBP4 localizes at site of inactive divisomes.
Figure S6. PBP4 localizes between the outer membrane and the peptidoglycan layer in a Δ*nlpI* strain.
Figure S7. Interactions of PBP4 and PBPP4ΔD3 measured by microscale thermophoresis (MST).
Figure S8. PBP4 or NlpI do not affect the activity of PBP1A or PBP1A/LpoA.
Figure S9. NG-FtsE effectively localizes and recruits PBP4.
Figure S10. PBP4 localization is not dependent on the presence of TolA, Pal, NlpD or AmiABC.
Table S1. Morphological parameters LMC500 and LMC500Δ*dacB*

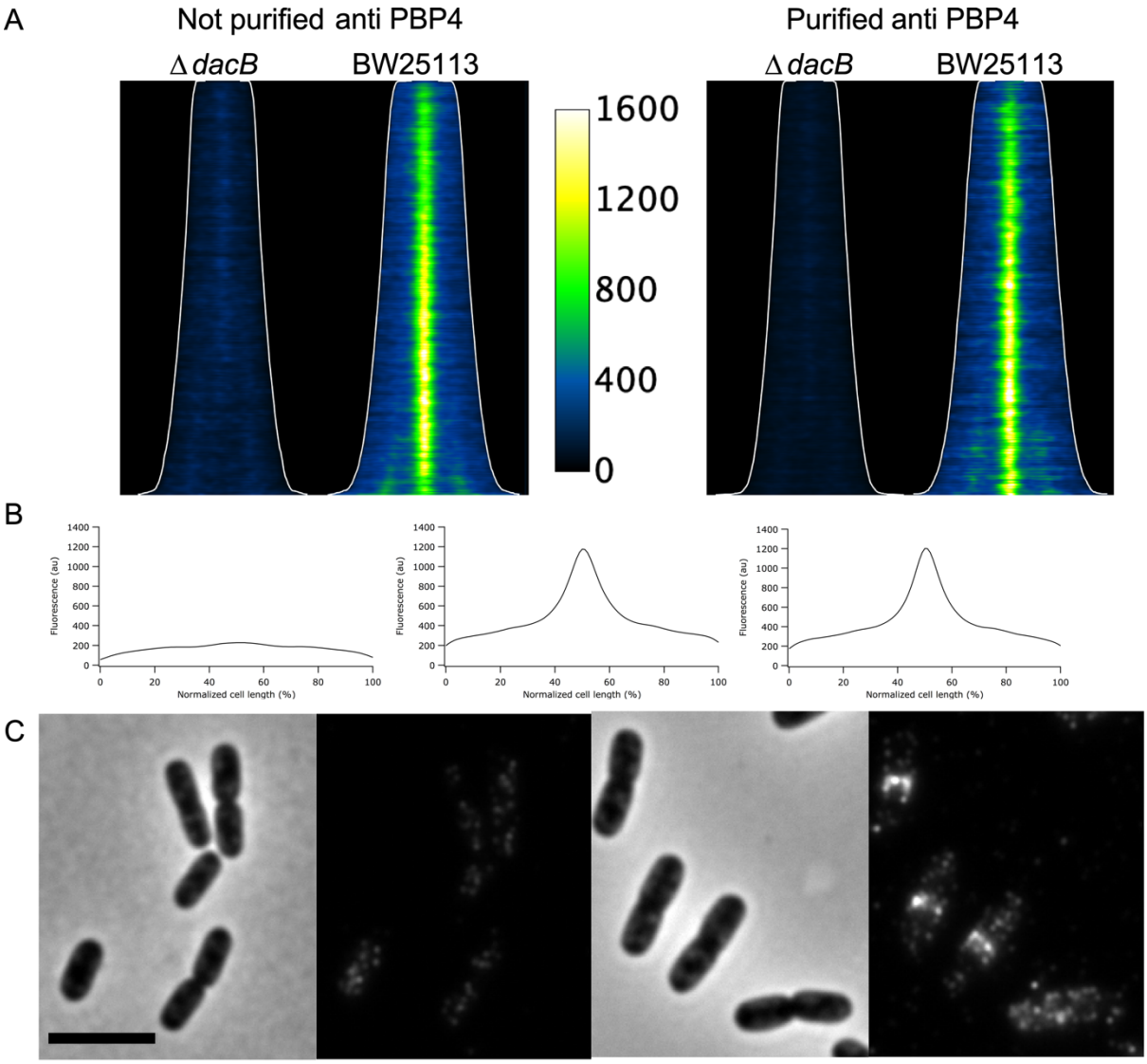

FIG S1 Pre-adsorption of antibodies against Δ*dacB* BW25113 strain results in PBP4 specific antibodies. (A) Demograph with cells sorted according to length of PBP4 fluorescence of the BW25113Δ*dacB* (PBP4) strain, BW245113 (wt) strain before purification of the antibody and the BW25113Δ*dacB* strain and BW245113 strain after purification of the antibody. (B) Absolute fluorescence average profiles of cells from the BW25113 Δ*dacB* strain and the BW245113 strain before purification of the antibody and from the BW245113 strain after purification of the antibody (C) Phase contrast and corresponding fluorescence image of anti PBP4 immunolabeled BW25113Δ*dacB* (left) and wild-type cells using the supernatant of BW25113Δ*dacB* pre-adsorbed antibodies. The scale bar equals 5 µm.

54

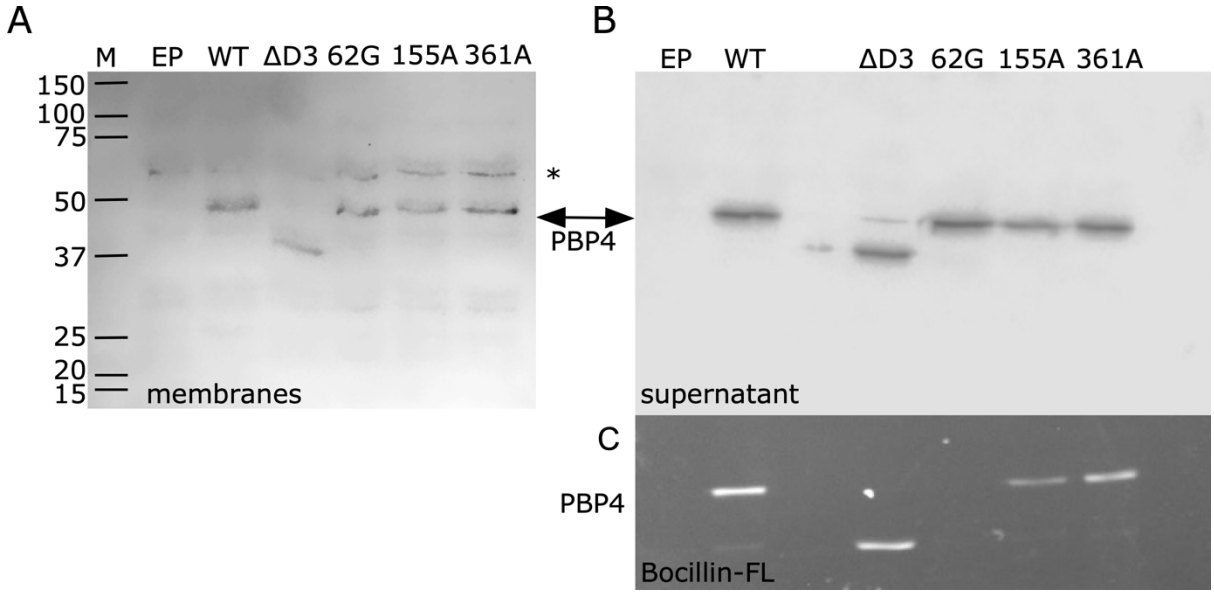

55

56

57 **FIG S2 All PBP4 mutants are equally well expressed and only S62G is not able to bind**

58 **Bocillin-FL. (**A) An immunoblot of membranes of PBP4 wild-type and variants. *This extra

59 band is due to non-specificity of the primary antibody, which was for the purpose of

60 immunoblotting not affinity purified. (B) Immunoblot of supernatant after pelleting the

61 membrane of PBP4 wild-type and variants. (C) The corresponding gel where binding of the

62 fluorescent β-lactam Bocillin-FL is visible for all mutants apart from S62G. EP is empty plasmid,

63 WT is wild-type. The other samples are PBP4 variants.

64

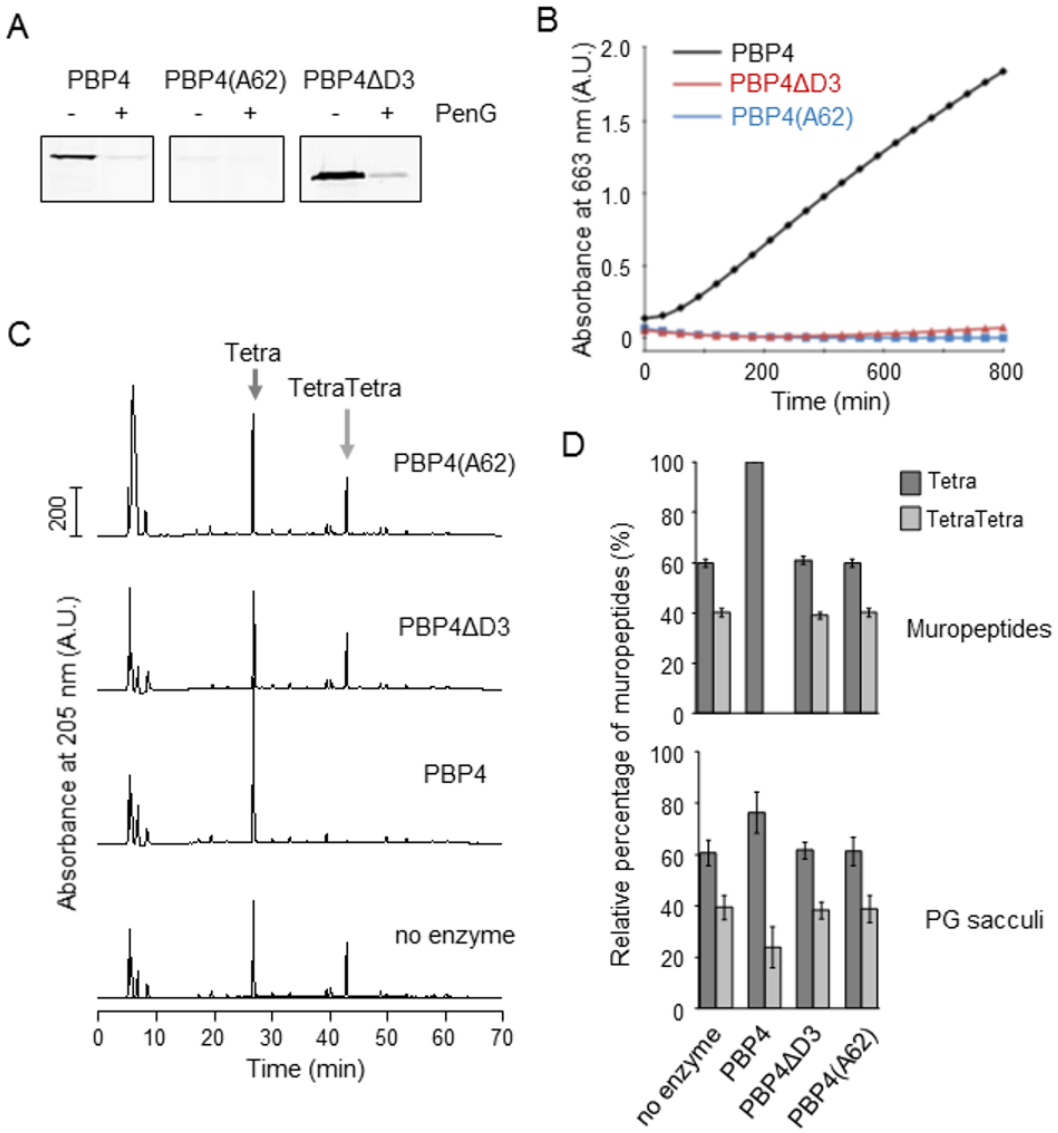

FIG S3 PBP4ΔD3 binds beta-lactam but is inactive against PG substrates. (A) PBP4 versions were incubated with the fluorescent β-lactam Bocillin FL with or without pre-incubation with Penicillin G (PenG), followed by SDS-PAGE analysis and detection of covalent Bocillin-PBP4

69 adducts by fluorescence scanner. PBP4 and PBPP4ΔD3, but not catalytically inactive
70 PBP4(S62A), bound Bocillin FL. (B) Only wild-type PBP4, but not PBPP4ΔD3 or PBP4(S62A),
71 was active in a DD-carboxypeptidase assay. (C) PBP4 versions were incubated with
72 muropeptides from BW25113 prior to their separation by high-performance liquid
73 chromatography (HPLC). A control sample contained no enzyme. PBP4 DD-endopeptidase
74 activity is demonstrated by the reduction in the dimer (TetraTetra) substrate peak and
75 increase in the monomer (Tetra) product peak. PBPP4ΔD3 and PBP4(S62G) were inactive. (D)
76 Quantification of the Tetra and TetraTetra peaks shown in panel C (top) and quantification of
77 a similar analysis with PG sacculi (incubated with PBP4 versions or no enzyme), followed by
78 generation of muropeptides and HPLC analysis (bottom).
79

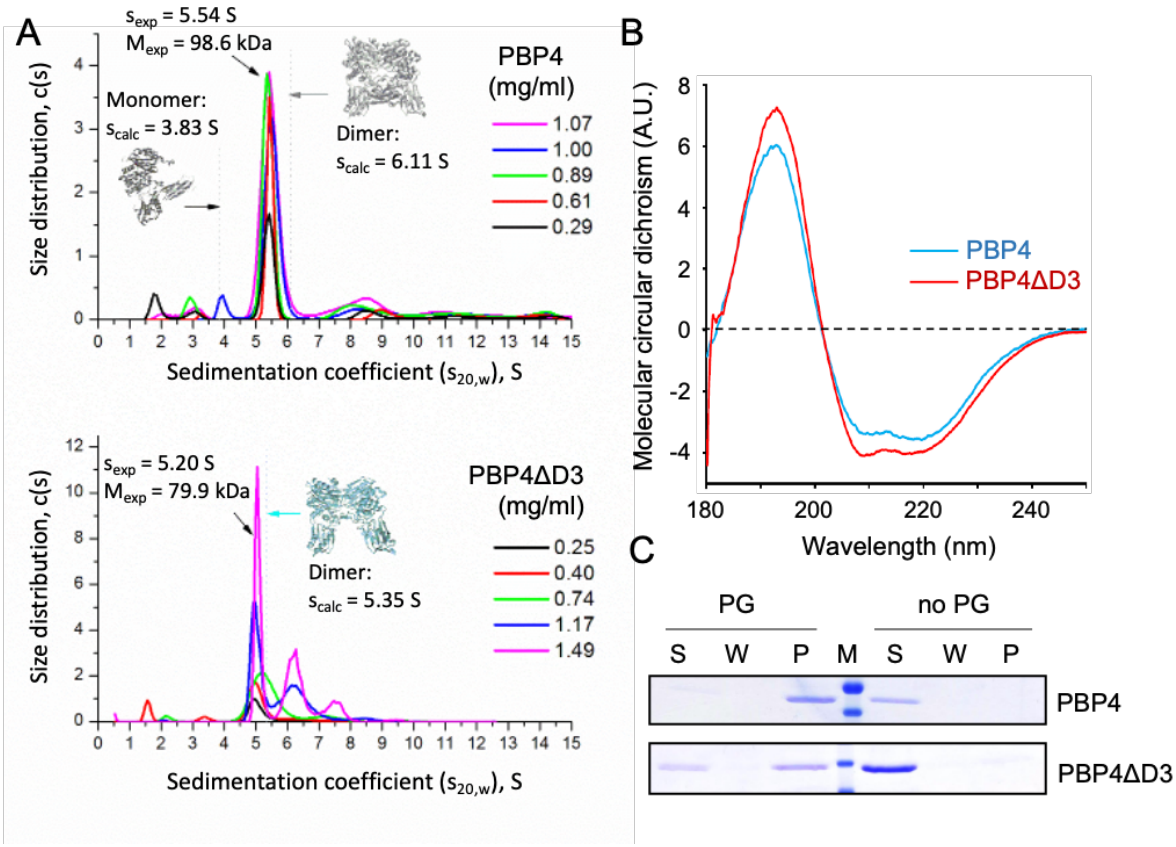

80

81 **FIG S4 The absence of domain 3 does not affect the dimerization, secondary structure or PG**
82 **binding of PBP4.** (A) Analytical ultracentrifugation sedimentation velocity experiment of PBP4
83 and PBP4ΔD3 shows that both proteins are mainly dimers. The determined sedimentation
84 coefficients (s_{exp}) for the dimers fit well with the theoretical values (s_{calc}) that were calculated
85 from atomic coordinates of both protein dimers (pdb accession code for monomer is 2EX2).
86 (B) PBP4 and PBP4ΔD3 show similar far UV circular dichroism spectra. (C) PBP4 and PBP4ΔD3
87 co-sediment with PG sacculi from BW25113 cells, but did not sediment in control samples
88 without sacculi, demonstrating binding to PG. S, supernatant; W, wash fraction; P, pellet
89 fraction.

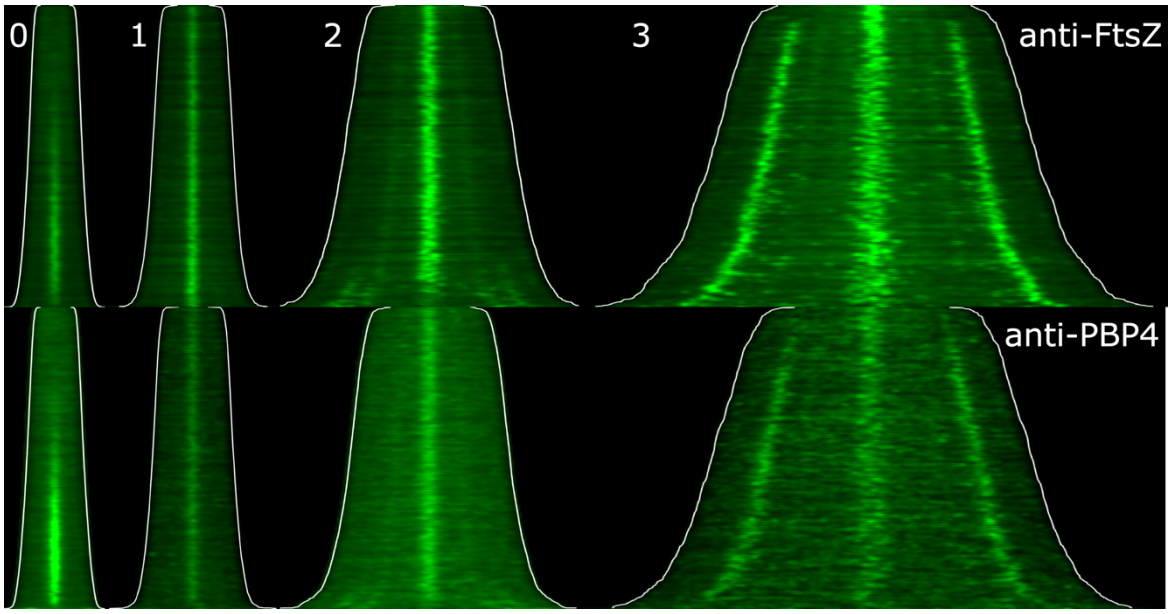

90

91 **FIG S5 PBP4 localizes at site of inactive divisomes.** MC4100 cells were grown to steady state
92 in minimal glucose medium at 28°C and split in two parts. One part was 1:4 diluted in
93 prewarmed medium without aztreonam and the other part was 1:4 diluted in medium with
94 10 µg/ml aztreonam. The cells continued to grow for 0, 1, 2 or 3 mass doublings (MD) and
95 were fixed and immunolabeled with antibodies specific for FtsZ or PBP4. Demographs with
96 identical brightness and contrast of the FtsZ or the PBP4 fluorescence of cells grown in the
97 absence or presence of aztreonam sorted according to length. The white line shows the

98 borders of the cells. Number of analyzed cells per demograph for FtsZ and PBP4 were, 5084

99 and 3448 (0), 1430 and 1858 (1), 857 and1630 (2) and 659 and 595 (3), respectively.

100

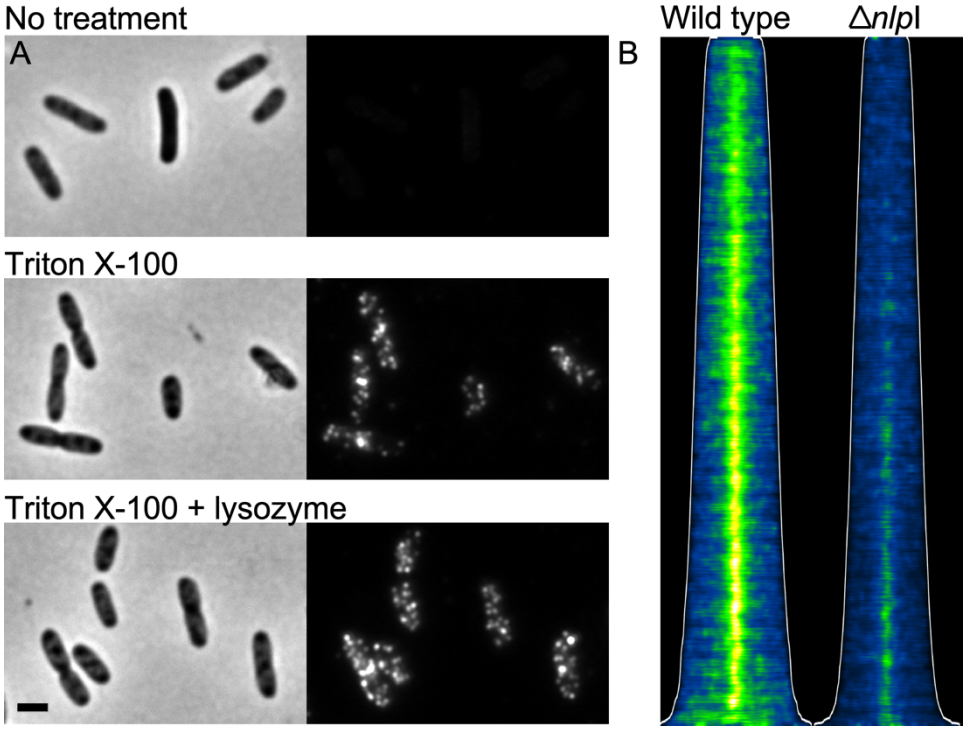

101

102 **FIG S6 PBP4 localizes between the outer membrane and the peptidoglycan layer in a Δ*nlpI***

103 **strain.** (A) BW 25113 Δ*nlpI* cells were grown exponentially in TY medium at 37°C and fixed

104 while shaking when at an OD600 of 0.3. The cells were harvested and split in three portions

105 of which one was directly immunolabeled with to Δ*dacB* cells pre-adsorbed anti-PBP4, the

106 second was first treated with Triton X-100 and the last was treated with Triton X-100 and

107 lysozyme and then immunolabeled. The scale bar equals 2 μm. (B) Map of PBP4 fluorescence

108 sorted according to cell length of wild-type cells and Δ*nlpI* cells displayed at the same

109 brightness and contrast values.

110

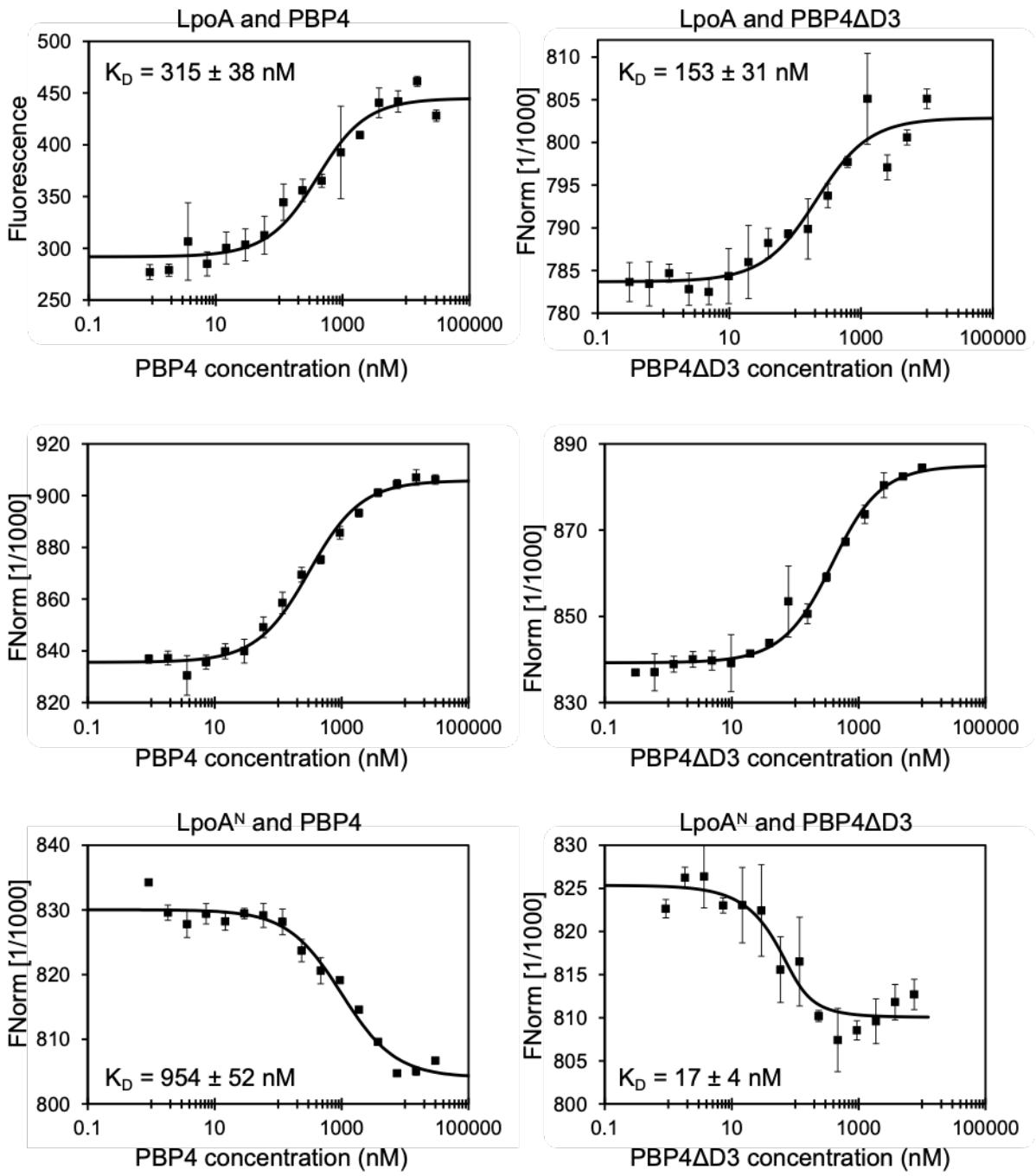
LpoA and PBP4
K_D = 315 ± 38 nM
Fluorescence
PBP4 concentration (nM)
LpoA and PBP4ΔD3
K_D = 153 ± 31 nM
FNorm [1/1000]
PBP4ΔD3 concentration (nM)
FNorm [1/1000]
PBP4 concentration (nM)
FNorm [1/1000]
PBP4ΔD3 concentration (nM)
LpoA^N and PBP4
K_D = 954 ± 52 nM
FNorm [1/1000]
PBP4 concentration (nM)
LpoA^N and PBP4ΔD3
K_D = 17 ± 4 nM
FNorm [1/1000]
PBP4ΔD3 concentration (nM)

111

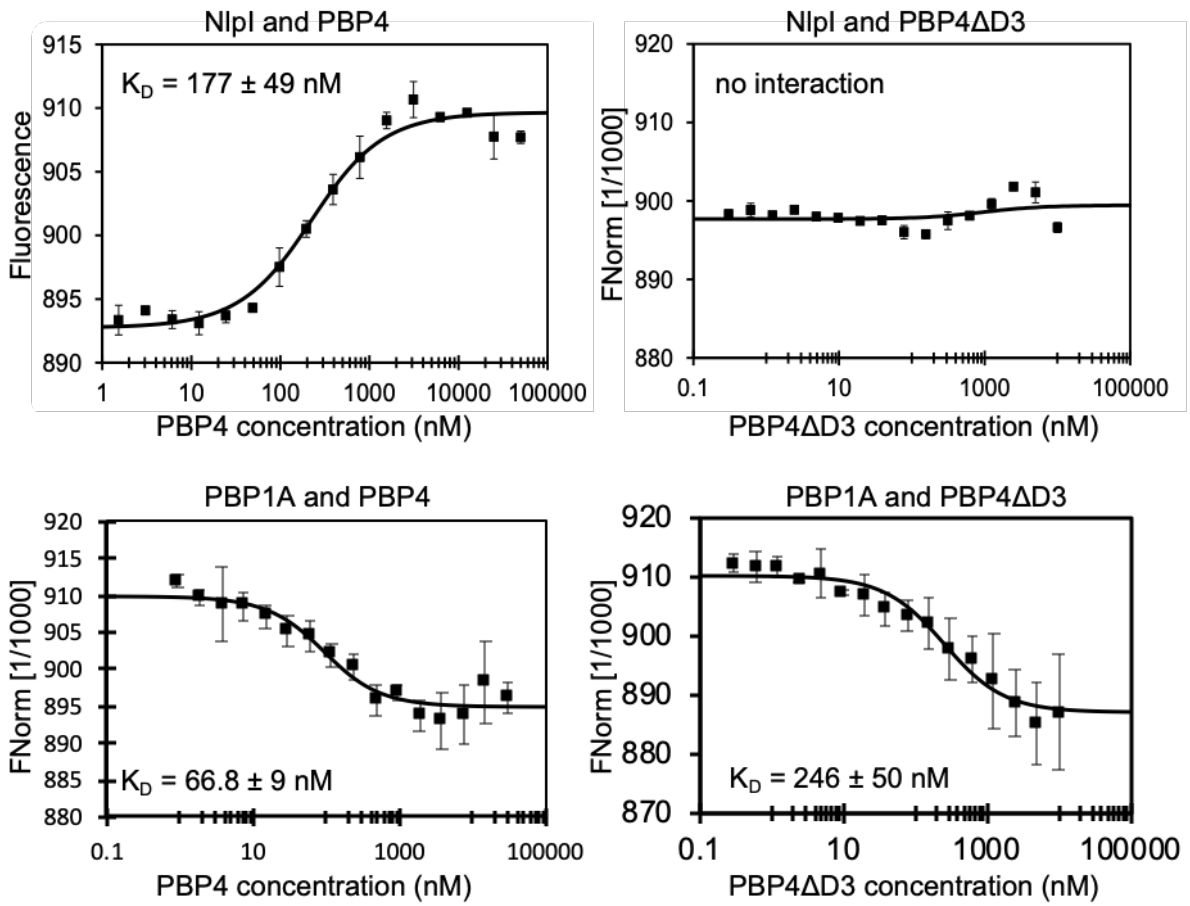

FIG S7 Interactions of PBP4 and PBPP4ΔD3 measured by microscale thermophoresis (MST). MST binding curves for interactions using different fluorescently-labelled proteins (LpoA, $LpoA^C$, Lpo^N, NlpI or PBP1A) titrated against fixed concentrations of PBP4 or PBPP4ΔD3. Apparent K_D values are mean ± SD of three independent experiments and summarized in Fig. 4A.

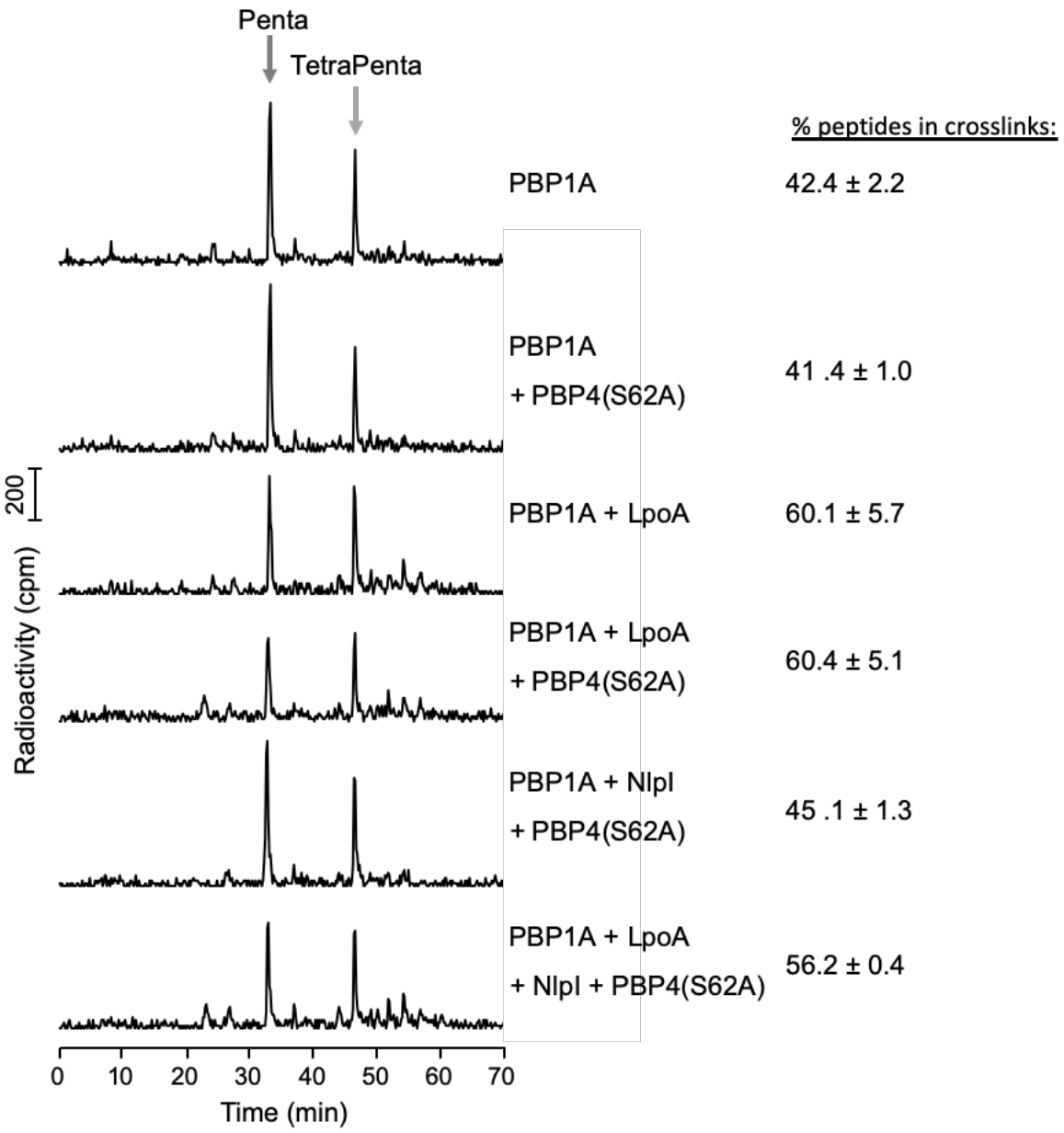

120

121

122 **FiG S8 PBP4 or NlpI do not affect the activity of PBP1A or PBP1A/LpoA.** Representative HPLC

123 chromatograms of samples from an *in vitro* PG synthesis assay of PBP1A and radiolabelled

124 lipid II, in the presence of proteins indicated. The main PG products upon digestion with the

125 muramidase cellosyl are the disaccharide pentapeptide (Penta) and the bis-disaccharide

126 tetrapentapeptide (TetraPenta). The % peptides present in cross-links is quantified on the

127 right side and presented as mean ± variation of two independent experiments.

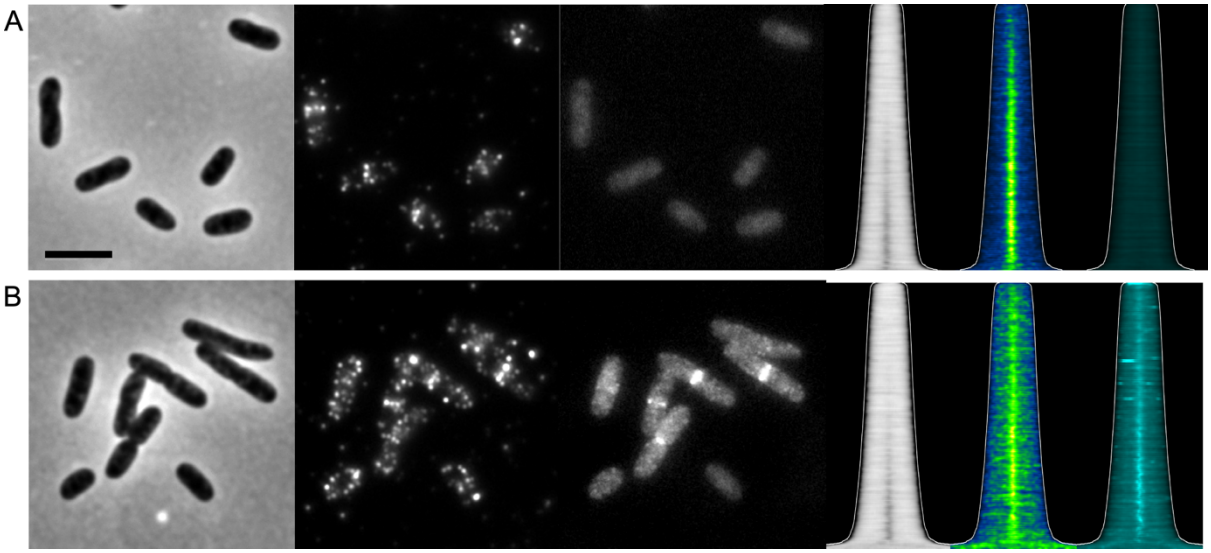

FIG S9 NG-FtsE effectively localizes and recruits PBP4. Strains were grown in LB at 37°C to an OD of 0.3 in the presence of 30 µM IPTG to induce expression of mNG-FtsE then fixed and immunolabeled with antibodies specific for PBP4. (A) LMC500 (1108 cells analyzed). (B) XL36 (LMC500::p*Trc*99down*ftsX*, Δ*ftsE*) with pXL110 mNG-FtsE(wt) (1189 cells analyzed). From left to right, phase contrast image, anti-PBP4 immunolabeling, mNG-FtsE, and the corresponding map of diameter with the fluorescence maps of cells sorted according to length. Scale bar equals 5 µm.

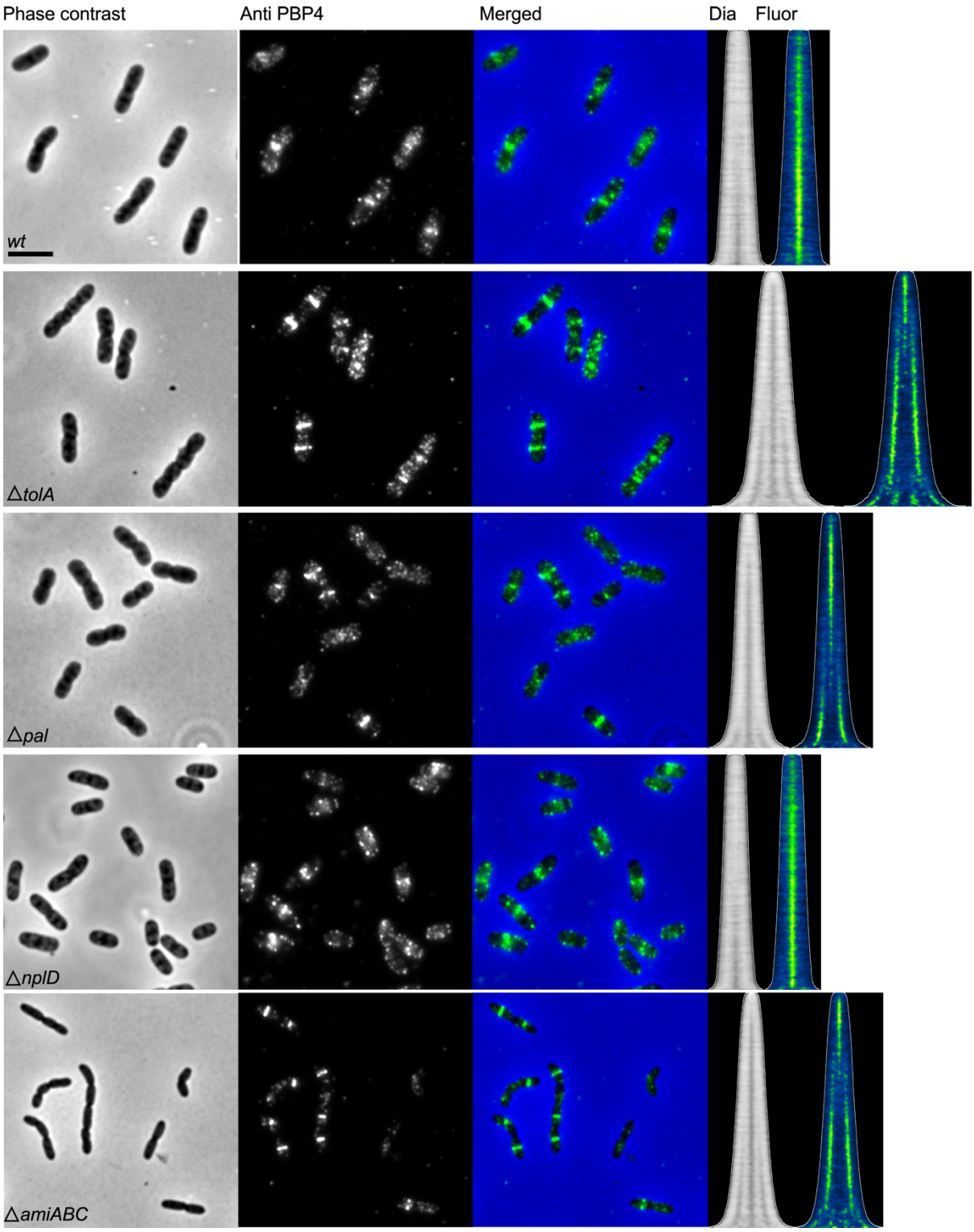

137

138 **FIG S10 PBP4 localization is not dependent on the presence of TolA, Pal, NlpD or AmiABC.**

139 Isogenic strains of the wild-type strain BW25113 were grown in LB at 37°C to a OD600 of 0.3,

140 fixed and labeled with specific antibodies against PBP4. From left to right, the phase contrast,

141 corresponding fluorescence image of the PBP4 labeling, and the merged former two images,

142 map of diameters (Dia) and map of fluorescence (Fluor) PBP4 localization where cells are
143 sorted according to their cell length are shown. The number of cells analyzed were 1053 for
144 BW25113 (*wt*), 918 for Δ*tolA*, 1314 for Δ*pal*, 1600 for Δ*nlpD*, and 1410 for Δ*amiABC*. The scale
145 bar equals 5 µm.
146
147 **Table S1. Morphological parameters LMC500 and LMC500Δ*dacB***

Parameter	**LMC500**	**n**	**LMC500Δ*dacB***	**n**	**p**
Length (µm)	2.57 ± 0.07	8	2.58 ± 0.09	12	0.79
Diameter (µm)	0.89 ± 0.09	8	0.91 ± 0.19	12	0.73
Constrictions (%)	16.9 ± 1.8	8	17.4 ± 1.3	12	0.53

148 n = number of biological replicates, P from a two tailed T-test to verify whether that the means
149 are significant different.
150
151
152